Ar-Ar dating of late Cenozoic basaltic volcanism in northern Syria: Implications for the history of incision by the River Euphrates and uplift of the northern Arabian Platform

Tuncer Demir,[1] Rob Westaway,[2,3] David Bridgland,[4] Malcolm Pringle,[5,6] Sema Yurtmen,[7,8] Anthony Beck,[9,10] and George Rowbotham[11]

Received 27 February 2006; revised 1 December 2006; accepted 19 February 2007; published 14 June 2007.

[1] Ar-Ar dating of basalt flows capping terrace deposits of the River Euphrates in northern Syria has provided a new quantitative chronology for the late Cenozoic evolution of this important river system and for the associated history of surface uplift of the northern Arabian Platform through which it flows, a region of relatively strong crust that has experienced only slow deformation. Notably, fluvial deposits ~65 m above the Euphrates are overlain by basalt dated to 2717 ± 20 ka, those ~45 m above the river are overlain by basalt dated to 2116 ± 39 ka, and those 8–9 m above the river are overlain by basalt dated to 402 ± 11 ka. These new dates require the previous dating scheme, based on Paleolithic archaeology, to be revised; the Euphrates terrace deposits and the associated incised valley are much older than was previously thought. Rates of incision by the Euphrates, providing a proxy for regional surface uplift that is inferred to be the isostatic response to regional erosion, have varied significantly over the past ~3 Ma, with indications that between ~1.2 and ~0.9 Ma, there was regional subsidence, which gave rise to fluvial aggradation. This unusual pattern, involving reversals in the sense of vertical crustal motions, is interpreted to be a consequence of a relatively cold and thin mobile lower crustal layer, no more than ~5 km thick, evidently due to the presence of a much thicker underlying layer of mafic underplating at the base of the crust. This study thus indicates previously unsuspected complexity in the isostatic response to regional erosion in an area of high crustal stability. **Citation:** Demir, T., R. Westaway, D. Bridgland, M. Pringle, S. Yurtmen, A. Beck, and G. Rowbotham (2007), Ar-Ar dating of late Cenozoic basaltic volcanism in northern Syria: Implications for the history of incision by the River Euphrates and uplift of the northern Arabian Platform, *Tectonics*, *26*, TC3012, doi:10.1029/2006TC001959.

1. Introduction

[2] This paper reports the first isotopic dating of the basaltic volcanism in northern Syria, at sites along the River Euphrates upstream of Deir ez-Zor (Figure 1). With a length of ~2800 km, the Euphrates (Fırat in Turkey; Furat in Syria) is the longest river in SW Asia. From its source in NE Turkey it flows initially west and south, then SE across the Arabian Platform (in SE Turkey, northern Syria and western Iraq; Figure 1) to the Persian Gulf, >1000 km downstream from the study region. The Arabian Platform was a marine depocenter within the Tethyan Sea (linking the Mediterranean Sea and Indian Ocean) until the middle late Miocene [e.g., *Lovelock*, 1984], although early middle Miocene fluvial sands and gravels are widespread near its northern margin around Kahramanmaraş [e.g., *Derman*, 1999] (Figure 1). Their diverse clast content, including metamorphic lithologies not found in situ in the Arabian Platform, indicates that a major river, draining at least part of the modern upper Euphrates catchment, debouched into the Tethyan Sea here at this time (stage 1 in Figure 1).

[3] Across much of the northern Arabian Platform, the transition from a marine depocenter to a subaerial landscape postdated the deposition of early Miocene marine limestone. Around Kahramanmaraş, it is marked by basaltic andesite volcanism, for which early middle Miocene K-Ar dates (all $\pm 2\sigma$) of 18.6 ± 0.8 Ma, 17.1 ± 0.8 Ma, 16.5 ± 0.6 Ma [*Arger et al.*, 2000], 19.1 ± 1.3 Ma and 17.0 ± 0.7 Ma [*Tatar et al.*, 2004] have been obtained. At some localities, notably (again) around Kahramanmaraş, fluvial gravels that were deposited at about this time interdigitate with shallow marine deposits and with lava flows [e.g., *Karig and Kozlu*, 1990; *Derman*, 1999], indicating the effect of cyclic changes in global sea level during emergence of the land surface. However, the crests of some anticlines are capped

[1]Department of Geography, Harran University, Şanlıurfa, Turkey.
[2]Faculty of Mathematics and Computing, Open University, Newcastle-upon-Tyne, UK.
[3]Also at School of Civil Engineering and Geosciences, Newcastle University, Newcastle-upon-Tyne, UK.
[4]Department of Geography, Durham University, Durham, UK.
[5]Scottish Universities' Environmental Research Centre, Glasgow, UK.
[6]Now at Laboratory for Noble Gas Geochronology, Department of Earth, Atmospheric, and Planetary Sciences, Massachusetts Institute of Technology, Cambridge, Massachusetts, USA.
[7]Department of Geology, Çukurova University, Adana, Turkey.
[8]Now at Newcastle-under-Lyme, UK.
[9]Department of Geography, Durham University, Durham, UK.
[10]Now at School of Computing, University of Leeds, Leeds, UK.
[11]School of Earth Sciences and Geography, Keele University, Keele, UK.

Copyright 2007 by the American Geophysical Union.
0278-7407/07/2006TC001959

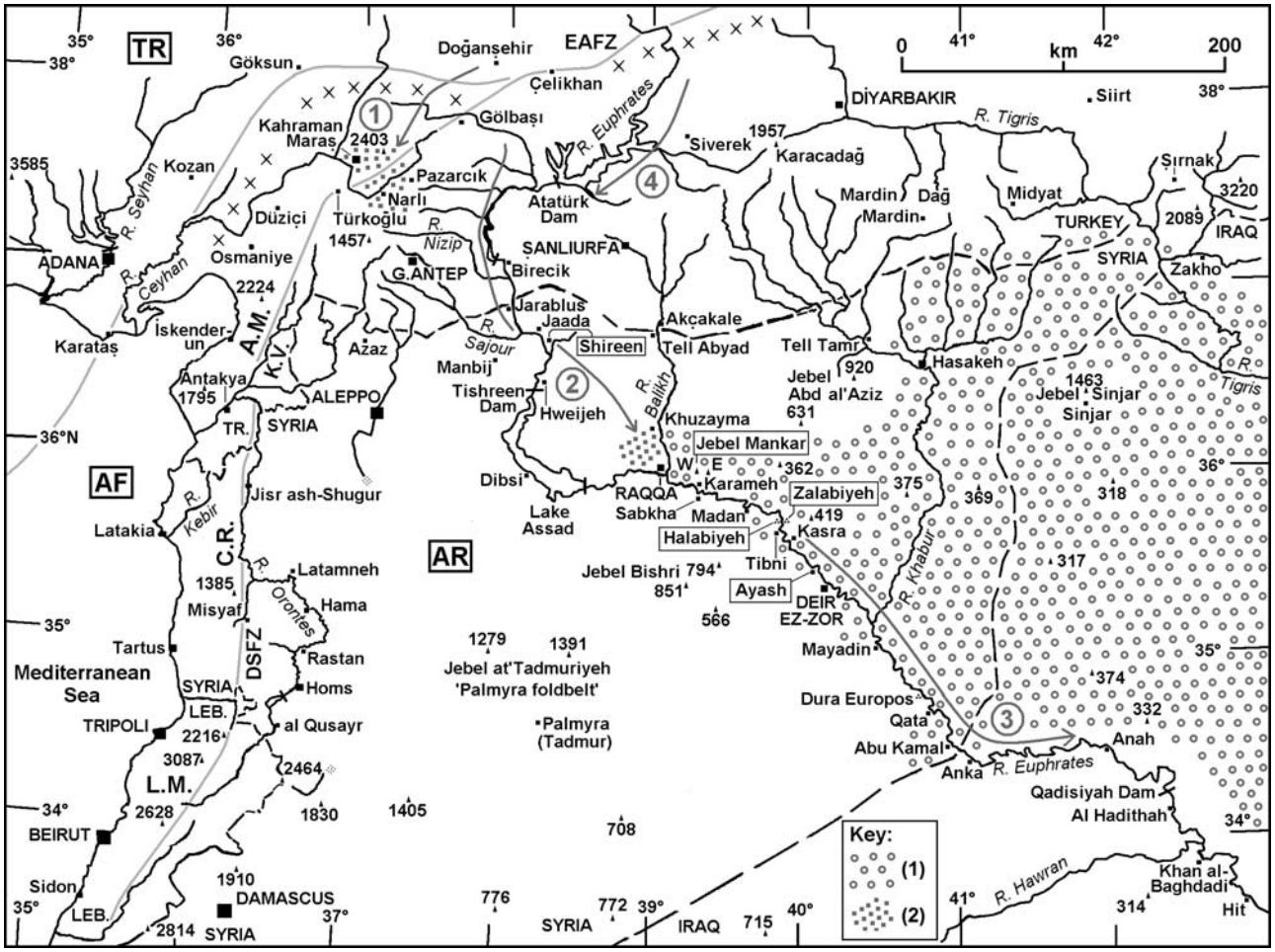


Figure 1. Regional map showing the location of the study area in relation to the River Euphrates and the active left-lateral strike-slip faults (simplified from *Westaway* [2004a]) bounding the Arabian (AR), African (AF), and Turkish (TR) plates. Boxed names are basalt sample localities. Mountain ranges forming as a result of transpression along the DSFZ are labeled as follows: L.M., Lebanon Mountains; C.R., Syrian Coastal Range (Jebel Nusayriyah); A.M., Amanos Mountains. K.V. denotes the Karasu Valley; crosses mark the suture of the Neotethys Ocean. 1, 2, 3, and 4 indicate the Euphrates courses inferred in the middle Miocene, late Miocene, Pliocene, and Pleistocene. In the legend, 1 indicates outcrop of the Upper Fars Formation; 2 indicates concentrations of stacked fluvial sand and gravel, from the early middle Miocene and (?) late Miocene.

by reef deposits of Oligocene or early Miocene age, implying local emergence above sea level earlier than for the landscape as a whole [e.g., *Rigo de Righi and Cortesini*, 1964]. Some of the largest of these mid-Cenozoic anticlines, overlying blind reverse faults, form the Mardin Dağ uplands in SE Turkey, the Jebel Bishri and Jebel Abd al-Aziz uplands in northern Syria, the Jebel Sinjar uplands in NW Iraq, and the Jebel at'Tadmuriyeh uplands or "Palmyra Foldbelt" in central Syria (Figure 1). Many other basalt flows that likewise postdate the regional emergence of northern Syria have been mapped [e.g., *Ponikarov and Mikhailov*, 1964], although none has previously been dated.

[4] Previous studies have revealed extensive Euphrates terrace deposits between Birecik in SE Turkey and the Syria-Iraq border [e.g., *Besançon and Sanlaville*, 1981; *Minzoni-Deroche and Sanlaville*, 1988; *Besançon and Geyer*, 2003], as well as farther downstream in Iraq [*Tyráček*, 1987]. In SE Turkey, the oldest and highest of these exceed 200 m above present river level. No direct age control evidence has been provided previously for any locality in this reach, although ages have been suggested for Euphrates terraces in Syria and southern Turkey as part of a regional correlation scheme based partly on Paleolithic artifact assemblages from the gravels. In western Iraq, *Tyráček* [1987] suggested that the observed change from a low-relief landscape to an increasingly entrenched river valley, as revealed by the geometry and disposition of the preserved terraces, marked the start of the middle Pleisto-

cene. This followed a similar interpretation by *Kukla* [1978] of a comparable landscape change that is evident from terrace records in central Europe.

[5] The disposition of the Euphrates terrace deposits evidently reflects changes in hydrology on Milankovitch or longer timescales, superimposed onto effects of regional uplift. By analogy with other fluvial sequences in the region [e.g., *Collier et al.*, 2000; *Demir et al.*, 2004; *Westaway et al.*, 2006b], it is considered that aggradation of these deposits occurred primarily at times of cold climate, when the reduction of vegetation cover in upstream parts of the catchment would have brought about increased influxes of sediment into the system and relatively low ratios of discharge to sediment load, as the rainfall during such cold stages is believed to have been relatively low. Conversely, during temperate climatic optima, increased vegetation cover would have restricted mass movement into the fluvial system and the associated higher rainfall would have resulted in a high ratio of discharge to sediment load. Such conditions would have enabled the river to incise, in response to the regional uplift, by which means progressively lower valley floors (terraces) would have formed. This mechanism for terrace formation, by cyclic climatic triggering in response to background uplift, has been widely advocated in recent years in areas rich in paleoenvironmental and dating evidence, such as NW Europe [e.g., *Maddy*, 1997; *Bridgland*, 2000; *Westaway*, 2002b; *Bridgland and Westaway*, 2007]. Marine base level control is seen as unimportant, excepting very close to coastlines [e.g., *Rose et al.*, 1999; *Macklin et al.*, 2002; cf. *Kiden and Törnqvist*, 1998].

[6] The aim of this paper is to present results of Ar-Ar dating of basalts interbedded with the fluvial sequence, thereby constraining the ages of the Euphrates terraces and, assuming the terraces to provide a record of fluvial incision, to use this evidence to deduce the history of vertical crustal motion in this part of northern Syria. In addition, geochemical analysis is used to classify the sampled basalts and to address the thermal state of the underlying crust and mantle lithosphere, knowledge of which is needed for the numerical modeling of the vertical crustal motions that then follows. The work has implications for the wider consideration of fluvial evolution in response to crustal deformation and climatic fluctuation, as well as the understanding of late Cenozoic landscape development in regions of relatively high crustal stability. Since the Euphrates deposits are repositories for Paleolithic artifacts [e.g., *Besançon and Sanlaville*, 1981; *Copeland*, 2004; *Sanlaville*, 2004], the work will also have implications for the understanding of human occupation in the Levant, which lies on the probable migration route between Africa and Eurasia.

2. Regional Background

2.1. Regional Tectonics

[7] Eastern Turkey forms the modern boundary zone between the African, Arabian, Eurasian, and Turkish plates. Westward motion of the Turkish plate relative to Eurasia and Arabia is being accommodated by right-lateral slip on the North Anatolian Fault Zone (NAFZ) and conjugate left-lateral slip on the East Anatolian Fault Zone (EAFZ; Figure 1). A promontory of the African plate persists northward through western Syria into central southern Turkey (reaching the vicinity of Kahramanmaraş; Figure 1), bounded relative to the Arabian plate by the Dead Sea Fault Zone (DSFZ) and relative to the Turkish plate by other left-lateral faults. The kinematics of these strike-slip fault zones are now well constrained by both GPS satellite geodesy and geological evidence [e.g., *McClusky et al.*, 2000; *Westaway*, 2003, 2004a; *Westaway et al.*, 2006a]. For much of their length these zones involve transform faulting, which requires no vertical component of crustal motion, but locally they delineate transpressive step overs, where local crustal shortening requires localized surface uplift in order to balance crustal volume [e.g., *Westaway*, 2003, 2004a; *Gomez et al.*, 2006] (Figure 1). This modern geometry of strike-slip faulting is thought to date from ~4 Ma [e.g., *Westaway*, 2003, 2004a; *Westaway et al.*, 2006a]; it is thought to have superseded an earlier, but similar, geometry of strike-slip faulting, which existed between ~7 and 4 Ma [e.g., *Westaway and Arger*, 2001]. Prior to this, this region accommodated northward (or northwestward) convergence of the African and Arabian plates relative to Eurasia.

[8] The NAFZ and EAFZ converge at the Karlıova "triple junction" in NE Turkey (~41° East). East of this point, Arabia-Eurasia convergence is accommodated directly, by active reverse faulting. Before the modern strike-slip fault systems developed, in the late Miocene and early Pliocene, active reverse faulting (and active folding of anticlines over blind reverse faults) was much more widespread in eastern Turkey and northern Syria. It is thought that many such structures became active in the late Eocene, at the start of the continental collision between Africa/Arabia and Eurasia; beforehand, the convergence between Africa and Eurasia was instead accommodated by northward subduction of the Southern Neotethys Ocean beneath Anatolia [e.g., *Aktaş and Robertson*, 1984]. The suture of this ocean (Figure 1; sometimes known as the Bitlis-Zagros suture), separating the Arabian Platform to the south from the Anatolian metamorphic terrane to the north, is the principal geological boundary in this region.

[9] Superimposed onto these effects of plate motions has been a component of regional uplift. As *Arger et al.* [2000] first noted, since the middle Miocene, when much of the Arabian Platform emerged above sea level, this has amounted to ~1000 m near the Neotethys suture and ~500 m or more in parts of the Arabian Platform interior near the Turkey-Syria border. Recent studies [e.g., *Arger et al.*, 2000; *Demir et al.*, 2004, 2007] indicate that this component of uplift has had nothing directly to do with plate motions, and seems instead to be the local manifestation of the systematic increase in relief that has developed within the continents during the late Cenozoic, apparently as a consequence of coupling between surface processes (such as erosion) and induced flow in the lower continental crust [e.g., *Westaway et al.*, 2003; *Bridgland and Westaway*,

2007] (see sections 3.4, 5.3, and 5.4). Regional uplift on the same timescale has been even more dramatic within eastern Anatolia, where early Miocene marine sediments are now found ~2 km or more above sea level [e.g., *Westaway and Arger*, 2001]. It is evident that several factors must be considered when reconstructing the evolution of the Euphrates: the local effects of faulting and folding, lateral variations in regional uplift, and the need to maintain a downstream channel gradient.

[10] As illustrated in Figure 1, the modern left-lateral strike-slip fault systems are located well to the west and north of the present study region. Before this modern geometry of strike-slip faulting developed, at ~4 Ma (3.73 ± 0.05 Ma according to *Westaway et al.* [2006a]), the relative motion between the Arabian and African plates seems to have been accommodated instead by a different system of faults located east of the modern DSFZ, some passing through the Gaziantep area of SE Turkey (Figure 1) and adjoining parts of Syria [e.g., *Chaimov et al.*, 1990; *Coşkun and Coşkun*, 2000; *Westaway*, 2003]. As will be discussed in more detail in section 5.3, the localized tilting of some of the older Euphrates deposits (notably around Halabiyeh; Figure 1) and the localized faulting of some of the underlying bedrock (notably, at Shireen; Figure 1) is inferred to date from this time.

2.2. Cenozoic Evolution of the Euphrates Catchment

[11] Most bedrock outcrops along the Euphrates in the vicinity of the Turkey-Syria border (Figure 1) consist of Cenozoic (upper Eocene to Oligocene) marine carbonates [*Ponikarov et al.*, 1967], during deposition of which the northern Arabian Platform was submerged beneath the Tethyan seaway linking the Mediterranean Sea and Indian Ocean. Unconformable Miocene marine limestone in northern Syria was assigned by *Ponikarov et al.* [1967] to the Jeribe Formation (equivalent to the Fırat Formation in SE Turkey [cf. *Terlemez et al.*, 1997]). This is a stratigraphic unit of regional significance, extending from Syria to Iran, dated to the early middle Miocene (Langhian [*James and Wynd*, 1965; *Alsharhan and Nairn*, 1995]). Diverse carbonate facies are evident, suggesting rapidly changing shallow marine conditions. This limestone is overlain by deposits assigned by *Ponikarov et al.* [1967] to the Lower Fars Formation, another regionally significant unit, of late middle Miocene (Burdigalian) age [*James and Wynd*, 1965; *Alsharhan and Nairn*, 1995]. Around Shireen (Figure 1) this consists of interbedded green calcareous clay and marl, red mudstone and white limestone with occasional gypsum layers, and is no more than a few tens of meters thick. Farther north, near the Turkish border, conglomerate and cross-bedded sandstone assigned to this unit indicate marginal marine conditions with input of clastic sediment from the north. By this time a land bridge connected Arabia with Turkey (between Aleppo and Gaziantep; Figure 1), isolating the Mediterranean Sea from the Mesopotamian Basin of Iran, Iraq and NE Syria.

[12] No younger stacked sediments are found in this area. However, east of Raqqa (Figure 1) there is extensive outcrop of the Upper Fars Formation, consisting of up to ~250 m of clay, siltstone, fine sandstone and gypsum. These deposits record a marine to lagoonal or lacustrine transition in the late Miocene [e.g., *James and Wynd*, 1965; *Alsharhan and Nairn*, 1995]. Younger stacked terrestrial sediments, assigned to the Pliocene and correlated with the Bakhtiari Formation of Iraq, also crop out widely in eastern Syria, notably around Deir ez-Zor. These consist of sand and gravel, with a general upward coarsening trend, with calcareous clay and gypsum interbeds [*Ponikarov et al.*, 1967], indicating a lacustrine depocenter with fluvial input. The gravel clasts include igneous (e.g., granite, peridotite) and metamorphic (e.g., quartzite, calc-schist, gneiss) rocks derived from Anatolia, indicating the existence at that time of an ancestral Euphrates (stage 3 in Figure 1).

[13] As with the other principal rivers of Syria, the Orontes (Aassi) and Kebir (Figure 1), the Euphrates sequence has been extensively researched by French workers principally interested in the Paleolithic archaeology contained in the deposits [e.g., *Besançon and Geyer*, 2003; *Copeland*, 2004; *Sanlaville*, 2004]. A uniform terrace classification and dating scheme was applied throughout, established first in the Orontes and Kebir and then extended to the Euphrates by *Besançon and Sanlaville* [1981]. This scheme recognizes five terraces, from QfV, the oldest, to QfI, the youngest (the Q standing for "Quaternary" and the f for "fluvial"). These have been assumed to be of the same age wherever recognized; typical heights above present river level of the tops of each of these terraces, as originally defined, are listed in Table 1. In addition, the most recent (latest Pleistocene and Holocene) deposits are designated Qf0, including the modern floodplain and older deposits, forming very low terraces, some of which aggraded during historical time. In contrast with the five terraces recognized in Syria by *Besançon and Geyer* [2003] and *Sanlaville* [2004], *Tyráček* [1987] identified 10 terraces above the Euphrates floodplain in Iraq.

[14] A degree of age constraint is provided by the relative disposition of the various terrace deposits of the Kebir, in NW Syria, in relation to marine (raised beach) sediments inland of Latakia (Figure 1). Furthermore, temperate stage deposits interbedded with cold stage gravels of terrace QfIII, ~60 m above the modern level of the middle Orontes at Latamneh, have yielded a mammal fauna that is suggestive of an age around 0.5 Ma [cf. *Bridgland et al.*, 2003]. Correlation between different valleys and between different reaches of the same valley has relied upon altitude above present river level, reinforced by artifact assemblages from the various terrace deposits. In the most recent appraisal of the Euphrates sequence, *Sanlaville* [2004] proposed that terrace QfV formed in MIS 18 and earlier, QfIV formed in MIS 16, QfIII in MIS 14 and/or 12, QfII in MIS 8, and QfI formed in MIS 6 and/or 4 (Table 1). However, the main basis of this scheme, the assumption that rates of vertical crustal motion do not vary laterally throughout Syria, has since been refuted. Notably, surface uplift in the parts of western Syria that have hitherto yielded the age control evidence is now known to relate in part to transpression along the DSFZ [e.g., *Westaway*, 2003, 2004a; *Gomez et al.*, 2006] (Figure 1). Thus, although Paleolithic artifacts, like

Table 1. Existing Terrace Scheme for the Raqqa–Deir ez-Zor Area[a]

Terrace	Height,[b] m	MIS[c]	Archaeology Classification[c]	Artifact Types[c]
Qf0	~1	2–1	Neolithic/historical	Neolithic and later
QfI	10–15	6 and/or 4	middle Paleolithic[d]	Levallois or "Levallois-like" material[d]
QfII	20–25	8	Upper Acheulian[d]	As QfIII but with hand axes; deep patina absent[d]
QfIII	50–60	14 or 12	middle Acheulian[d]	flakes, cores, "choppers," "picks"; hand axes absent; deep brown patina[d]
QfIV	80	16	none[e]	none[e]
QfV	>100	18 or earlier	none	none

[a]This is a summary of the existing correlation and dating scheme for the Euphrates terraces in the Raqqa–Deir ez-Zor area, advocated by previous workers [e.g., *Besançon and Sanlaville*, 1981; *Sanlaville*, 2004].

[b]Typical altitude above present river level of the upper surface of the terrace deposits.

[c]After *Sanlaville* [2004] and/or *Copeland* [2004].

[d]In the upstream reaches referred to in note 3, assemblages with hand axes are reported from deposits attributed (on the basis of height) to QfIII and assemblages with Levallois or Levallois-like material are reported from QfII [cf. *Copeland*, 2004]. The miscorrelation suggested by the height-driven interpretation on which this terrace scheme is based can be explained if the surface uplift has tapered southward, toward the interior of the Arabian Platform, as others [e.g., *Arger et al.*, 2000] have previously inferred, and is also indicated by the analysis in the present study.

[e]In the Manbij/Birecik region farther upstream (toward and beyond the Turkish border), assemblages of flakes and cores (Lower Acheulian/Khattabian) occur in the terrace designated QfIV [e.g., *Copeland*, 2004].

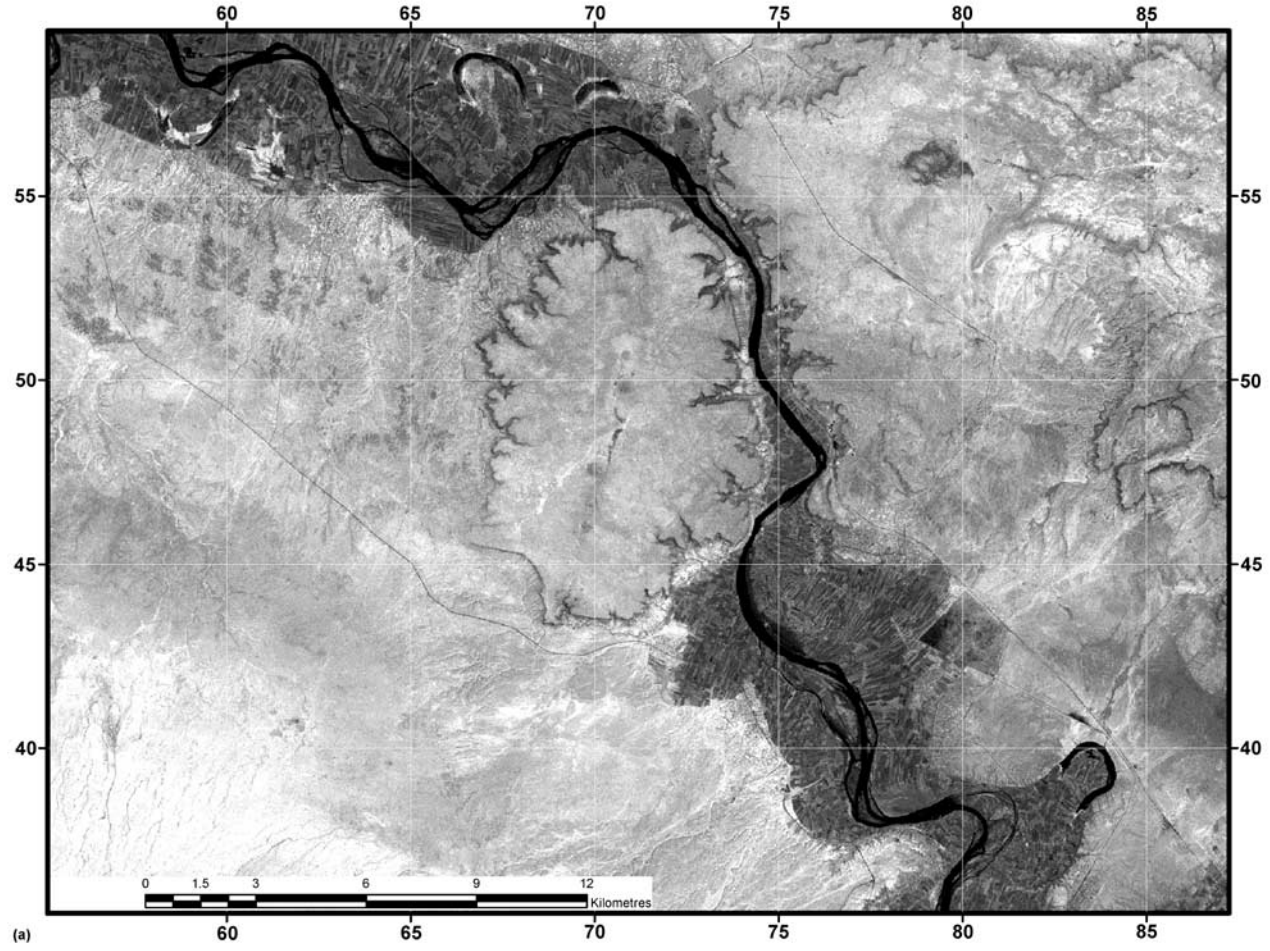


Figure 2a. Landsat ETM+ image covering the Halabiyeh and Zalabiyeh plateaus (Figures 1 and 3b). This image has been projected into the Universal Transverse Mercator (UTM) coordinate system using the WGS84 reference frame. Adjoining the Zalabiyeh Plateau to the east is the larger (~15 by ~20 km) basalt-capped Kasra Plateau. The local basalt appears to have emerged from a neck, Jebel as-Samman, reaching 419 m asl, shown in Figure 1.

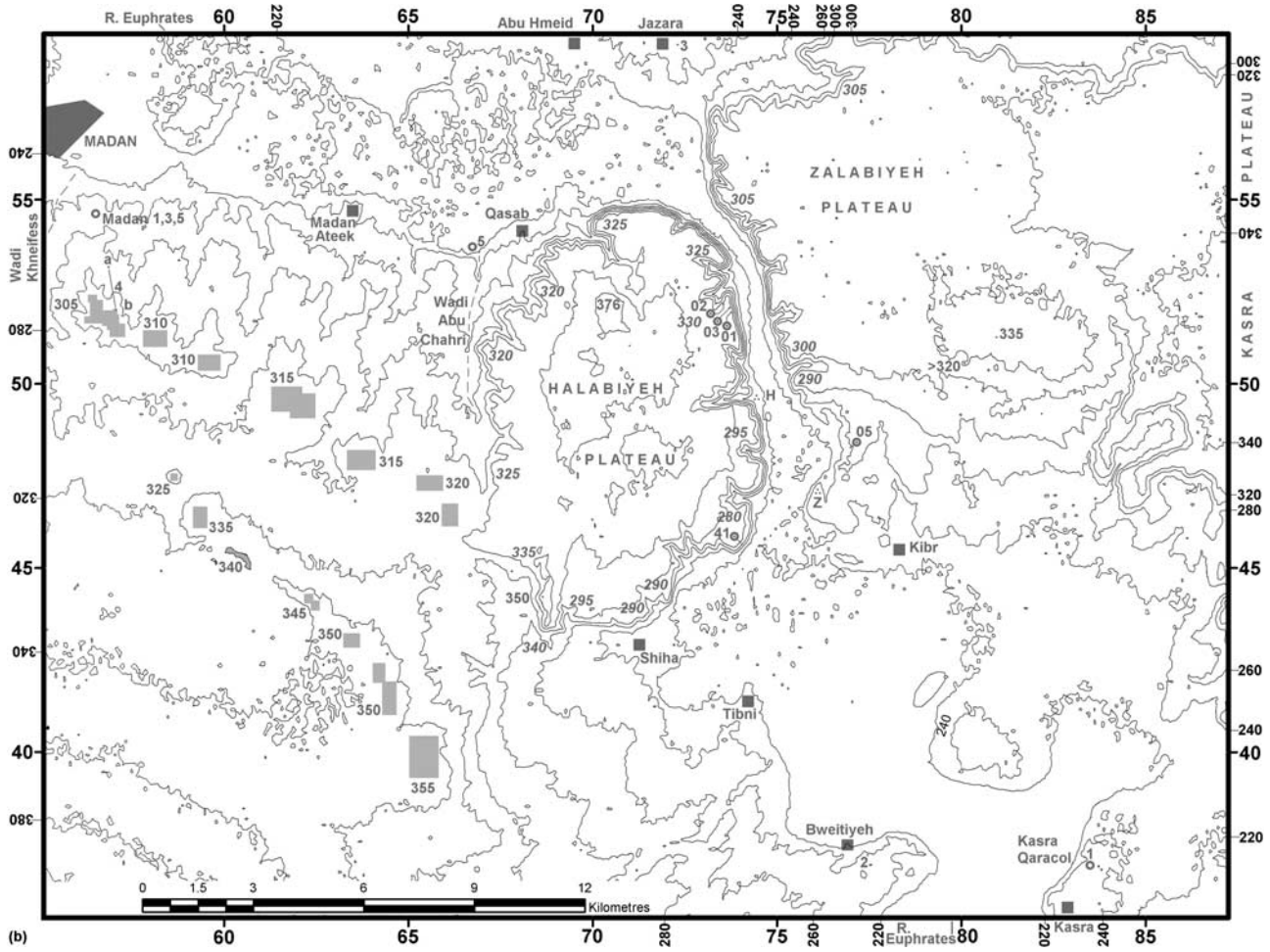


Figure 2b. Contour map with labeled 20 m contours, derived from SRTM imagery, covering the Halabiyeh and Zalabiyeh plateaus (Figures 1 and 3b), displayed using the same coordinate system and reference frame as Figure 2a. The auxiliary material includes another SRTM topographic image of this area, with 5 m contours.

any other form of trace fossil, can have age diagnostic significance [e.g., *Bridgland et al.*, 2006; *Westaway et al.*, 2006c], no a priori assumptions are made here about the ages of any of the artifact assemblages that have previously been reported in the Euphrates.

3. Methods

3.1. Terrace Mapping

[15] The accurate location of key sites has utilized Landsat imagery (Figure 2a). Surface heights have been measured (Figure 2b) using Shuttle Radar Topographic Mission (SRTM) interferometric radar altimetry data [e.g., *Rabus et al.*, 2003]. These two types of imagery were obtained and processed as described by *Westaway et al.* [2006a], details that are also summarized in the auxiliary material. The nominal horizontal precision of any point imaged by SRTM is ±20 m [*Jet Propulsion Laboratory*, 1998, available online at http://www2.jpl.nasa.gov/srtm/factsheet_tech.pdf]. The nominal vertical precision is much greater, but previous studies [e.g., *Miliaresis and Paraschou*, 2005; *Westaway et al.*, 2006b] have reported discrepancies (i.e., combinations of components of systematic and random error) of ~10 m or

Figure 3. Maps of the Euphrates terraces between Raqqa and Deir ez-Zor (Figure 1), adapted from Figure 6 of *Demir et al.* [2007] with permission, based on map 1 of *Besançon and Sanlaville* [1981]. (a) The reach around Raqqa. The modern Wadi al-Khar now drains the western part of the Raqqa paleomeander loop, flowing south toward the modern Euphrates, the opposite direction to that inferred for the flow of the Euphrates when it occupied this loop. (b) The reach around Halabiyeh. (c) The reach between Bweitiyeh and Deir ez-Zor. Chronological terms are those used by *Besançon and Sanlaville* [1981] and in subsequent studies such as by *Sanlaville* [2004]; see Table 1 for modern MIS equivalents, although the new Ar-Ar dating indicates that these ages are underestimates.

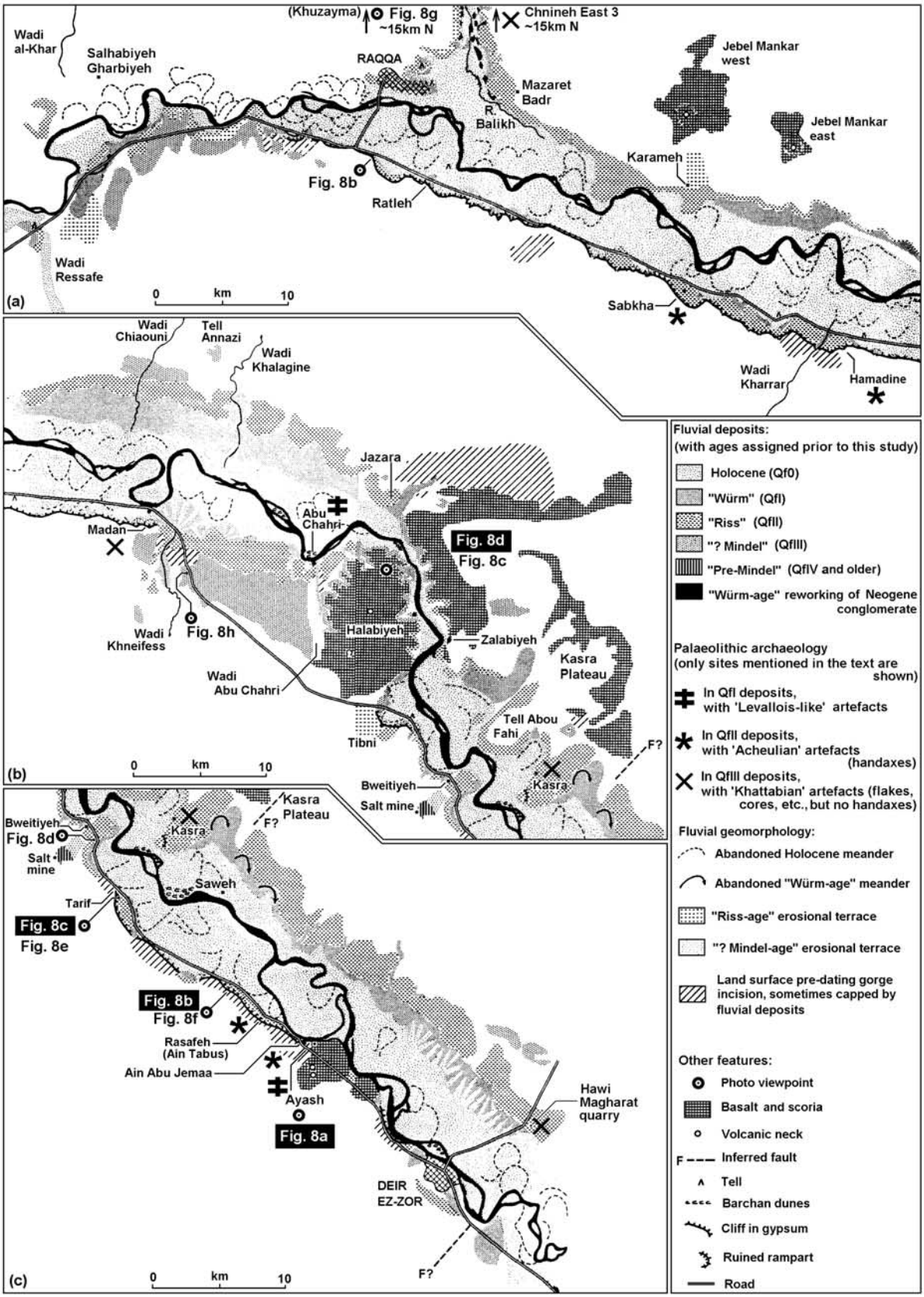

(Khuzayma)
Fig. 8g
~15km N
Chnineh East 3
~15km N
Wadi al-Khar
Salhabiyeh Gharbiyeh
RAQQA
Mazaret Badr
R. Balikh
Jebel Mankar west
Jebel Mankar east
Karameh
Fig. 8b
Ratleh
Wadi Ressafe
(a)
0 km 10
Sabkha
Wadi Chiaouni
Tell Annazi
Wadi Khalagine
Wadi Kharrar
Hamadine
Jazara
Abu Chahri
Madan
Fig. 8d
Fig. 8c
Wadi Khneifess
Fig. 8h
Halabiyeh
Zalabiyeh
Kasra Plateau
Wadi Abu Chahri
Tell Abou Fahi
Tibni
F?
(b)
0 km 10
Bweitiyeh
Salt mine
Kasra
Kasra Plateau
F?
Bweitiyeh
Fig. 8d
Salt mine
Saweh
Tarif
Fig. 8c
Fig. 8e
Fig. 8b
Fig. 8f
Rasafeh (Ain Tabus)
Ain Abu Jemaa
Ayash
Fig. 8a
Hawi Magharat quarry
DEIR EZ-ZOR
F?
(c)
0 km 10
Fluvial deposits:
(with ages assigned prior to this study)
Holocene (Qf0)
"Würm" (Qfl)
"Riss" (QfII)
"? Mindel" (QfIII)
"Pre-Mindel" (QfIV and older)
"Würm-age" reworking of Neogene conglomerate
Palaeolithic archaeology
(only sites mentioned in the text are shown)
In Qfl deposits, with 'Levallois-like' artefacts
In QfII deposits, with 'Acheulian' artefacts (handaxes)
In QfIII deposits, with 'Khattabian' artefacts (flakes, cores, etc., but no handaxes)
Fluvial geomorphology:
Abandoned Holocene meander
Abandoned "Würm-age" meander
"Riss-age" erosional terrace
"? Mindel-age" erosional terrace
Land surface pre-dating gorge incision, sometimes capped by fluvial deposits
Other features:
Photo viewpoint
Basalt and scoria
Volcanic neck
Inferred fault
Tell
Barchan dunes
Cliff in gypsum
Ruined rampart
Road

Figure 3

more between SRTM altitudes and those measured on high-precision large-scale topographic maps, which means that the SRTM-derived altitudes used in this paper are subject to some uncertainty and require future verification. Use has also been made of previous terrace (geomorphological) mapping [e.g., *Besançon and Sanlaville*, 1981; *Oguchi*, 2001] (Figure 3) and general geological mapping at 1:1,000,000 scale by *Ponikarov and Mikhailov* [1964]. Site locations will be quoted using Universal Transverse Mercator (UTM) coordinates, in which the initial two letters denote the 100 × 100 km quadrangle, the following numbers represent distances east and north of the SW corner of this quadrangle. Figure 2b illustrates SRTM imagery of the central part of the study region with 20 m contour resolution. Imagery of the same area with 5 m contour resolution is provided in the auxiliary material.[1]

3.2. Isotopic Dating

[17] Basalt samples were collected from five localities adjoining the Euphrates, at Shireen, Jebel Mankar West, Halabiyeh, Zalabiyeh, and Ayash (Figure 1), for Ar-Ar dating in the Laboratory for Noble Gas Geochronology, Massachusetts Institute of Technology. The samples were crushed, washed in deionized water and dilute hydrochloric acid, sieved to a 60–80 μm size fraction, and phenocrysts and xenocrysts were removed by magnetic separation and hand picking. Following irradiation, argon isotopes were measured in the microcrystalline groundmass, using procedures essentially the same as those described by *Singer and Pringle* [1996] and *Harford et al.* [2002]. Results of this dating, which are summarized in Figure 4 and Table 2, are documented in full in the auxiliary material.

[18] Two splits of sample 03SY03 from Halabiyeh were dated, yielding ages of 2764.8 ± 29.3 ka and 2676.4 ± 27.2 ka (both $\pm 2\sigma$, Figures 4a and 4b). These splits are concordant at the $\pm 3\sigma$ level, suggesting that random error, rather than systematic error in either split, is probably the main cause of the difference between their numerical ages. A weighted mean age of both splits can thus be derived: 2717.3 ± 19.9 ka ($\pm 2\sigma$), which is taken to be the definitive age for this sample. Two splits of sample 03SY04, from Ayash, were also dated, yielding ages of 410.6 ± 14.6 ka and 389.5 ± 17.0 ka (both $\pm 2\sigma$, Figures 4c and 4d). These splits are concordant at the $\pm 2\sigma$ level, again suggesting that random error is the main cause of their different numerical ages. Again, a weighted mean age of both splits can be regarded as the definitive age for this sample: 401.6 ± 11.1 ka ($\pm 2\sigma$). For each of the other three samples, only a single split was analyzed (Figures 4e–4h).

3.3. Geochemical Analysis

[19] In addition to dating, geochemical analysis is used to classify the sampled basalts and to address the thermal state of the underlying crust and mantle lithosphere, knowledge of which is needed for the numerical modeling of the vertical crustal motions. To facilitate classification, whole rock samples were analyzed using an automated ARL 8420 X-ray fluorescence spectrometer at the School of Earth Sciences and Geography, Keele University. Major oxide analyses used fused glass beads with a 1:5 ratio of sample powder and lithium metaborate flux; trace element analyses used pressed powder pellets. For analytic details, see *Floyd and Castillo* [1992]; for details of calibration, see *Yurtmen et al.* [2002]. Table 3 lists the results of this analysis.

[20] Using total alkali versus silica content, most of the samples can be classified [after *Le Bas et al.*, 1986] as basanites (Figure 5). However, sample 03SY09 from Shireen is a picrobasalt, whereas the three from Jebel Mankar West (two samples of lava, 03SY07 and 08; and one of scoria, 03SY06, all with SiO_2 wt % ~40%) fall within the foidite classification field. In terms of normative composition, these samples are all alkali olivine basalt (using the definition of *Middlemost* [1985]), due to the presence of normative olivine and nepheline and the absence of normative quartz (Table 3). The highly mafic samples from Jebel Mankar West also contain normative leucite (Table 3).

[21] Overall, major and trace element abundances and interelement ratios of these samples (Table 3) are similar to many other intraplate (e.g., ocean island and continental rift) basalts [e.g., *Basaltic Volcanism Study Project*, 1981, *Fitton*, 1987; *Weaver et al.*, 1987]. The low ratios of Ba/La, <~10 in most cases (Table 3), suggest that crustal contamination of these basaltic magmas has been minimal. Many other characteristics suggest that they are the products of small-degree partial melting of asthenospheric material. Examples include the high (>~800 ppm) abundances of Sr, an element that is strongly concentrated in small-degree partial melt, and the low (~4) Zr/Nb ratios (Table 3). This ratio provides a measure of this effect, primarily because Nb becomes concentrated in the melt to a greater extent than Zr [e.g., *Johnson et al.*, 1989; *Camp and Roobol*, 1992]. However, fractional crystallization, rather than partial melting, could also explain some characteristics of these basalts. Major element compositions in many basaltic lavas are indeed largely controlled by removal or accumulation of the assemblage olivine + clinopyroxene + plagioclase + Fe-Ti oxide [e.g., *Weaver et al.*, 1987]. The presence of the olivine + plagioclase + augite + Ti-magnetite phenocryst assemblage, observed in thin sections, thus suggests that the magmas may have experienced low-pressure (<1.5 GPa) crystal fractionation [e.g., *Cox*, 1980].

[22] To assess the relative importance of partial melting and fractional crystallization, the abundances of Cr have been plotted against Y [after *Pearce et al.*, 1990]. The incompatible element Y becomes strongly concentrated in small-degree partial melt and is not readily taken up during any subsequent fractional crystallization. The compatible element Cr exhibits the opposite behavior: its tendency to remain bound within silicate crystal lattices means that it is strongly depleted in partial melt and becomes even more depleted in the residual melt left after any fractional crystallization. As Figure 6 indicates, the abundances of Cr and Y measured in the Syrian basalts indicate that small-degree partial melting was followed by only minimal

[1] Auxiliary material data sets are available at ftp://ftp.agu.org/apend/tc/2006tc001959. Other auxiliary material files are in the HTML.

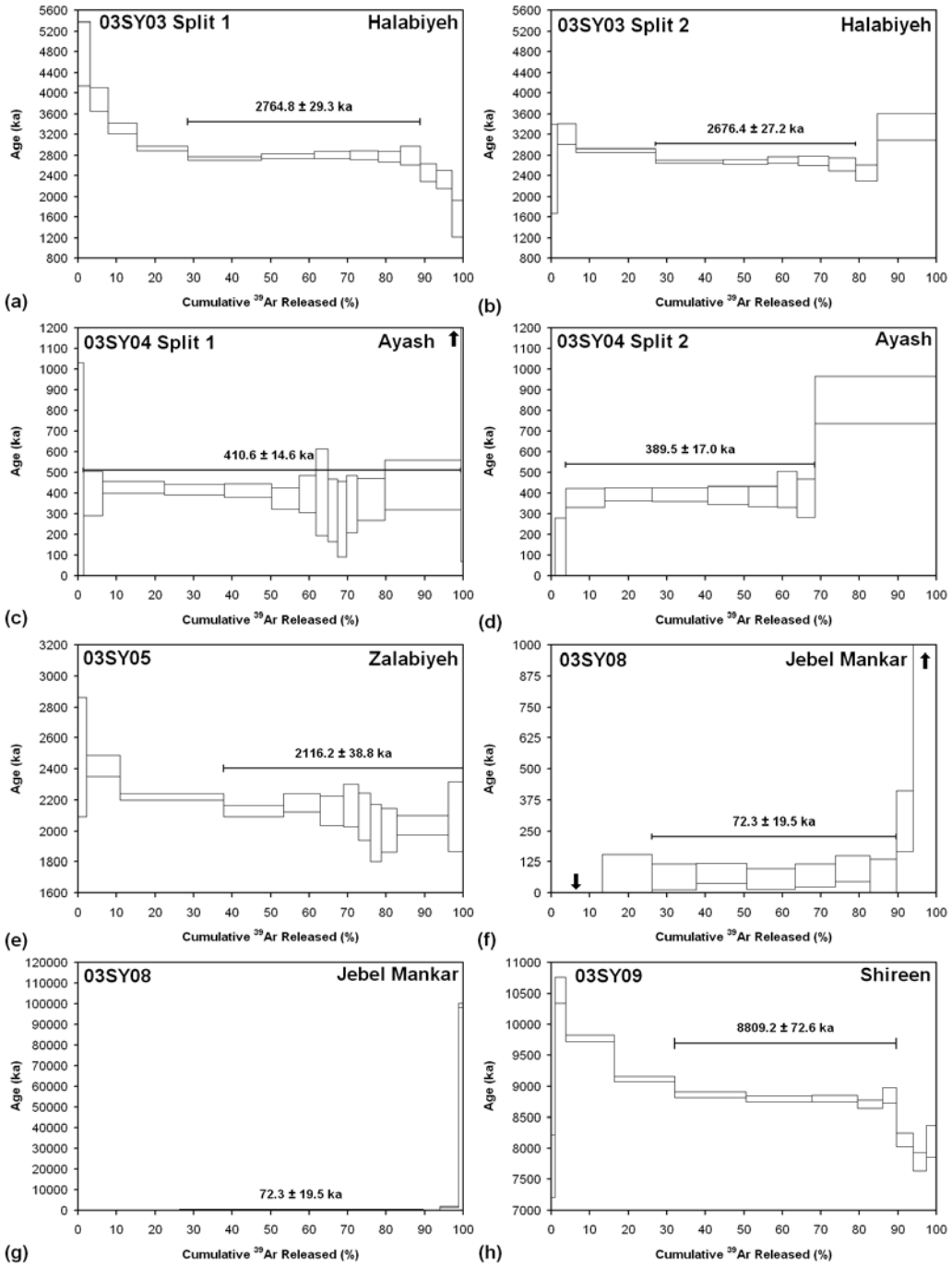


Figure 4. Graphs showing apparent Ar-Ar ages and their uncertainties for each heating step of each sample split. Horizontal bars indicate the splits that contribute to each of the ''weighted plateau'' age determinations in Table 2. Vertical arrows in Figures 4c and 4f indicate heating step apparent ages that fall outside the range being displayed. To better illustrate this effect, the results for sample 03SY08 have been displayed twice, over two different age ranges, in Figures 4f and 4g.

subsequent differentiation along fractional crystallization trends.

3.4. Uplift Modeling

[23] On the basis of the new dating control presented in sections 4.1, 4.2, and 4.3, the uplift history of the study reach of the Euphrates has been modeled, using the technique of *Westaway* [2001] and *Westaway et al.* [2002]. This technique, based on the assumption that the observed surface uplift is the isostatic consequence of net inflow of lower crust to beneath the study region, induced by surface processes, has been applied to many other fluvial sequences

Table 2. Summary of Results of Ar-Ar Dating[a]

Sample	Locality	UTM Coordinates	Split ID/Lab Number	Standard	$^{40}Ar(r)/^{39}Ar(k)$ ($\pm2\sigma$)	Age ($\pm2\sigma$), ka	MSWD	$^{39}Ar(k)$,%	n/N	K/Ca ($\pm2\sigma$)
03SY03	Halabiyeh	EV 73745 51948	A4/RW5F041A	tcr-2a	4.7988 ± 0.0421 (±0.88%)	2764.8 ± 29.3 (±1.06%)	1.05	60.41	6/13	0.772 ± 0.012
			C34/RW5F043C	tcr-2a	4.5167 ± 0.0372 (±0.82%)	2676.4 ± 27.2 (±1.02%)	0.56	51.94	5/10	0.713 ± 0.233
03SY04	Ayash	EV 94614 20938	A5/RW5F041B	tcr-2a	0.7196 ± 0.0252 (±3.50%)	410.6 ± 14.6 (±3.55%)	0.87	97.97	12/14	0.654 ± 0.009
			C35/RW5F043E	tcr-2a	0.6627 ± 0.0286 (±4.31%)	389.5 ± 17.0 (±4.35%)	0.18	64.63	7/10	0.876 ± 0.012
03SY05	Zalabiyeh	EV 76896 48300	A6/RW5F041D	tcr-2a	3.7511 ± 0.0651 (±1.74%)	2116.2 ± 38.8 (±1.84%)	2.10	62.16	9/12	0.580 ± 0.008
03SY08	Jebel Mankar W.	EV 23861 76044	A7/RW5F041E	fc-1	0.1297 ± 0.0350 (±27.01%)	72.3 ± 19.5 (±27.02%)	0.35	62.61	6/12	2.431 ± 0.119
03SY09	Shireen	DA 37571 47645	A8/RW5F041F	tcr-2a	16.0593 ± 0.0911(±0.57%)	8809.2 ± 72.6 (±0.82%)	3.98	57.57	5/12	0.642 ± 0.008

[a]All samples were of basaltic groundmass, separated as described in the text. Results listed are for the weighted plateau age determinations in Figure 4. Total fusion, normal isochron, and inverse isochron ages have also been determined for all samples; see the auxiliary material for details (the auxiliary material also provides full documentation of measurements not included in this table). "Standard" indicates the neutron flux monitor used: tcr-2a denotes the Taylor Creek Rhyolite tcr-2a sanidine standard, with an assigned age of 28.34 Ma [*Renne et al.*, 1998]; fc-1 denotes the Fish Canyon Tuff fc-1 sanidine standard, with an assigned age of 28.02 Ma [*Renne et al.*, 1998]. The $^{40}Ar(r)/^{39}Ar(k)$ is the measured ratio of the number of ^{40}Ar atoms produced by radioactive decay of the potassium in the sample to the number of ^{39}Ar atoms produced by irradiation of the potassium in the sample. MSWD is the mean squared weighted deviation, a measure of the scatter between individual age estimates for different heating steps. The $^{39}Ar(k)$ (%) is the percentage of the ^{39}Ar in the irradiated sample that is determined to have been produced by irradiation of potassium. K/Ca is the measured ratio of potassium to calcium atoms in the sample, which is used to correct the ^{39}Ar measurements for ^{39}Ar produced by irradiation of calcium. Age calculations assume decay constants from *Steiger and Jäger* [1977]. N is the total of heating steps measured; n is the number of these steps that were used for each age determination, as illustrated in Figure 4.

worldwide [e.g., *Westaway*, 2002b, 2004c; *Westaway et al.*, 2004, 2006b, 2006c; *Bridgland and Westaway*, 2007]. More detailed explanations have been provided elsewhere [e.g., *Westaway*, 2001, 2002a, 2002b, 2004b; *Westaway et al.*, 2002] and so are not repeated here. The fact that the Euphrates terraces are subparallel to each other and to the modern river gradient (see sections 4.1, 4.2, and 4.3) justifies the use of fluvial incision as a proxy for regional uplift in this system, since it demonstrates that down cutting has been a response to regional rather than differential uplift [cf. *Westaway et al.*, 2002]. This modeling technique assumes that the observed uplift is the net isostatic response to repeated cycles of loading and unloading of the crust, for instance by ice sheets or fluctuations in eustatic sea level. In general, increases in rates of erosion caused by global climate change can also induce net inward lower crustal flow [e.g., *Westaway*, 2002c]. Both mechanisms will in general occur together and their individual contributions can be difficult to resolve [*Westaway*, 2002a]. In the eastern Mediterranean region, however, it is likely that the observed uplift is primarily the isostatic response to increased rates of erosion [e.g., *Westaway et al.*, 2004]. Nonetheless, tests [e.g., *Westaway*, 2002a; *Westaway et al.*, 2004] have established that very similar uplift responses can result from both mechanisms whereby surface processes are coupled to induced lower crustal flow (i.e., from cyclic surface loading or from increased rates of erosion). The chosen technique, which is simpler to implement, requires fewer model parameters to be specified and can handle multiple phases of lower crustal flow forcing (LCFF), is thus used here as an approximation. The parameters to be specified are the magnitude ΔT_e and start time t_o of each phase of LCFF, the geothermal gradient u and thermal diffusivity κ of the lower crust, and W_i, a measure of the thickness of this mobile lower crustal layer.

4. Results

[24] Sites are discussed in geographical order, working upstream from Deir ez-Zor past Raqqa to the vicinity of the Turkish border (Figure 1). Figure 7 summarizes the evidence now available from sites that are discussed in the reach immediately upstream of Deir ez-Zor.

4.1. Deir ez-Zor Area

[25] At Ayash, ~10 km NW of Deir ez-Zor (Figures 1 and 3c), a young basalt flow, emanating from the nearby Hajif Shemali neck south of the Euphrates, has capped fluvial deposits, assigned to terrace QfI, that reach ~8–9 m above river level (Figures 8a and 9a). These deposits consist of gravel, up to ~3 m of which is exposed, overlain by ~6 m of yellow silt [*Perves*, 1964; *Besançon and Geyer*, 2003, p. 41]. *Besançon and Geyer* [2003] attributed the gravel here to MIS 6 or 4, based on the occurrence of what they refer to as "Late Levalloiso–Mousterian" artifacts at the top of the gravel. *Ponikarov and Mikhailov* [1964] estimated a late Pleistocene age for the basalt from its appearance in outcrop.

Table 3. Results of Geochemical Analysis[a]

	Northeast Syria										Diyarbakır Area	
	02SY41	03SY01	03SY02	03SY03	03SY04	03SY05	03SY06	03SY07	03SY08	03SY09	03TR61	03TR62
Coordinates												
	EV	EV	EV	EV	EV	EV	EV	EV	EV	DA	FB	FB
	74018	73697	73507	73745	94614	76784	23844	23851	23861	37571	08750	08750
	45596	52086	52223	51948	20938	48315	76091	76090	76044	47645	96004	96004
Major Elements, wt %												
SiO_2	42.76	42.93	41.83	42.62	44.08	44.84	40.61	39.49	39.88	44.14	46.32	46.88
TiO_2	3.63	3.47	3.50	3.47	2.87	3.33	3.14	3.28	3.35	2.73	2.54	2.47
Al_2O_3	12.29	11.88	12.33	12.21	11.98	12.21	9.93	9.89	10.41	11.94	14.12	13.79
Fe_2O_3T	14.76	14.43	14.89	14.69	13.52	15.24	13.92	14.13	13.93	13.00	14.57	14.01
MnO	0.17	0.17	0.17	0.17	0.17	0.18	0.18	0.18	0.18	0.16	0.16	0.15
MgO	11.19	11.46	12.24	11.77	12.00	11.22	15.46	16.26	15.10	10.09	9.16	9.56
CaO	10.58	10.77	11.07	10.82	10.54	11.29	11.10	11.57	11.56	12.02	8.73	8.82
Na_2O	3.16	2.49	2.29	2.42	3.43	2.98	3.44	3.67	4.15	1.94	2.92	2.78
K_2O	1.2	1.19	1.23	1.16	1.25	0.95	1.42	1.01	1.14	0.93	1.10	1.14
P_2O_5	0.47	0.53	0.58	0.56	0.66	0.59	0.90	0.87	0.91	0.48	0.39	0.37
LOI	0.26	0.49	0.68	0.67	−0.19	0.81	0.26	0.10	0.09	2.74	0.32	0.59
Total	100.47	99.81	100.80	100.55	100.31	100.67	100.36	100.47	100.69	100.17	100.32	100.56
Trace Elements, ppm												
Cr	311	346	359	356	339	333	495	445	352	291	307	305
Cu	103	105	107	108	93	100	88	74	81	86	93	93
Ga	22	24	21	24	21	24	20	18	23	19	22	21
Nb	37	42	41	43	46	42	66	65	69	42	25	24
Ni	255	242	251	253	269	243	398	384	290	229	222	232
Pb	5	5	10	1	3	6	8	2	2	12	4	4
Rb	12	11	10	9	13	9	14	10	13	8	7	12
Sr	805	949	1245	2077	794	1016	1006	889	998	755	746	738
Th	0	0	1	0	1	1	2	0	1	3	0	0
V	255	262	256	258	210	228	231	232	227	205	198	193
Y	23	20	20	21	26	22	26	26	27	23	20	21
Zn	104	105	105	108	109	118	116	109	109	99	111	113
Zr	192	193	190	174	198	204	240	248	253	177	146	143
Ba	686	262	214	235	208	296	106	323	336	207	165	293
Ce	46	35	64	35	69	58	99	107	116	42	42	23
La	29	41	25	35	35	27	57	50	52	27	14	20
Nd	34	18	41	26	37	33	48	48	53	25	28	13
Cl	293	126	169	211	309	63	418	167	284	154	42	27
S	300	171	120	94	598	151	188	82	119	85	190	91
Ratios												
Ba/La	23.66	6.39	8.56	6.71	5.94	10.96	1.86	6.46	6.46	7.67	11.79	14.65
Zr/Nb	5.19	4.60	4.63	4.05	4.30	4.86	3.64	3.82	3.67	4.21	5.84	5.96
Norms, wt %												
Ne	11.44	7.332	8.915	7.527	11.60	8.189	15.77	16.82	19.02	2.337	1.258	0.102
Ol	21.45	22.18	24.12	23.42	22.39	21.83	28.31	31.61	28.50	18.22	23.23	23.14
Le	0	0	0	0	0	0	6.580	4.680	5.283	0	0	0

[a]LOI means loss on ignition. Ne, Ol, and Le are abbreviations for normative nepheline, olivine, and leucite. Norm calculations assume a Fe_2O_3/FeO ratio of 0.2 wt % [*Middlemost*, 1989].

[26] Sample 03SY04 was collected from the exposure of the northern tip of this basalt flow, forming the bluff at the inner edge of Euphrates right-bank terrace Qf0 (Figure 8a). As noted in section 3.2, Ar-Ar dating has yielded a weighted mean age, from two splits of this sample, of 402 ± 11 ka (±2σ, Figures 4c and 4d). The deposits forming terrace QfI in this locality are thus much older than previously thought [cf. *Sanlaville*, 2004]. These deposits are also significantly older than those of Euphrates terrace QfI in the Birecik area, ~400 km farther upstream (Figure 1), which *Kuzucuoğlu et al.* [2004] have assigned to MIS 6.

[27] The type locality for Euphrates terrace QfII, the Abu Jemaa Formation of *Besançon and Sanlaville* [1981], is just upstream of Ayash (Ain Abu Jemaa; Figure 1). As illustrated in Figures 8b and 8c, the exposure of QfII deposits in this area, which has yielded hand axes [e.g., *Copeland*, 2004], consists of ~5 m of gravel overlain by up to ~10 m of loam. *Besançon and Geyer* [2003] reported the local altitude of the top of this loam as ~23 m above the present river level (Figure 9a); the top of the underlying gravel is thus taken as ~13 m above the river (Figure 7). Given this higher altitude than that of terrace QfI, the Ayash Ar-Ar date

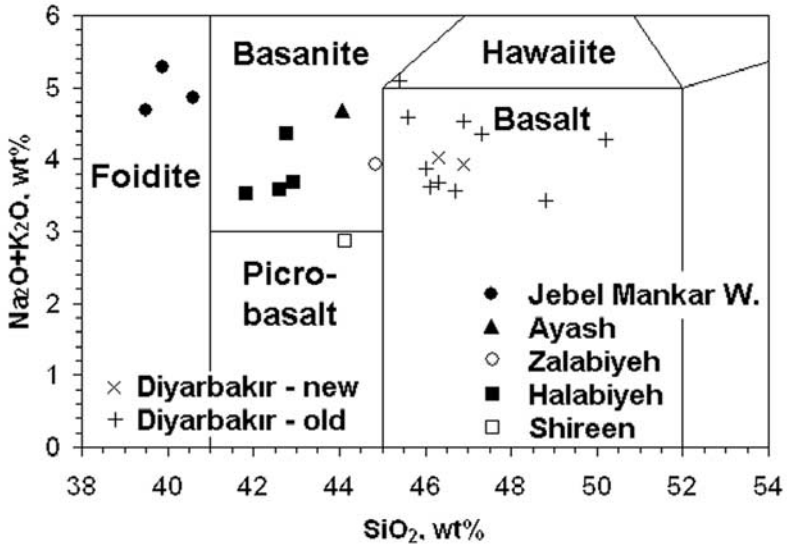


Figure 5. Total alkali ($Na_2O + K_2O$) versus SiO_2 diagram for Arabian Platform basalts [after *Le Bas et al.*, 1986].

makes it clear that terrace QfII in this region is older than MIS 12 and thus much older than the MIS 8 age previously inferred [cf. *Sanlaville*, 2004]. According to the archaeological dating scheme (Table 1), the different artifact assemblages reported in the QfI deposits at Ayash and the QfII deposits at Ain Abu Jemaa require the former to be younger than the latter [e.g., *Copeland*, 2004].

[28] At Hawi Magharat (~7 km NE of Deir ez-Zor; Figure 3c), sections in a gravel quarry reveal ~4 m of coarse polymict fluvial gravel with sand lenses, overlain by ~2 m of beige silt, capped by a thin gypsum crust [e.g., *Besançon and Geyer*, 2003; *Copeland*, 2004; *Sanlaville*, 2004]. The top of this section reaches ~210–215 m above sea level (asl), ~10–15 m above the present local level of the Euphrates. These fluvial deposits were grouped as part of terrace QfII by *Besançon and Sanlaville* [1981], as shown in Figure 3c, but have since been reclassified as part of terrace QfIII on the basis of the characteristics of the artifact finds, which include "picks," flakes and cores, most strongly patinated, but not hand axes [e.g., *Besançon and Geyer*, 2003; *Copeland*, 2004] (Figure 7). Given their altitude, the Ayash Ar-Ar date makes it clear that the deposits and associated artifacts of this terrace are also considerably older than the MIS 12 age previously envisaged [cf. *Sanlaville*, 2004].

4.2. Halabiyeh Plateau and Its Surroundings

[29] The ruined ancient walled city of Halabiyeh, on the right bank of the Euphrates, gives its name to the adjoining ~12 by ~8 km basalt plateau (Figures 2b and 3b). In the first detailed account of this locality, *Ponikarov et al.* [1967] reported that the basalt exposed in the plateau margin bluff is ~330 m asl (~120 m above the present river), ~12 m thick, and caps ~4 m of Euphrates gravel. In contrast, *Besançon and Geyer* [2003] described ~5 m of basalt, reaching ~70 m above the present river and capping ~10 m of fluvial gravel (Figures 8d and 9b). The SRTM imagery now reveals that different parts of the plateau margin are at different heights, indicating that the overlying basalt covers Euphrates gravels at a range of levels (Figure 2b). The *Ponikarov et al.* [1967] cross section (illustrated by *Demir et al.* [2007]) appears appropriate for the NE plateau margin (around the points where basalt samples 03SY01, 02 and 03 were collected), where the plateau margin is about at its highest, whereas the *Besançon and Geyer* [2003] cross section (Figure 9b) seems appropriate for the SE plateau margin (opposite Zalabiyeh, near where basalt sample 02SY41 was collected), where the plateau margin seems to be at its lowest.

[30] The observed lateral variations in altitude of the plateau margins are illustrated in Figure 2b. Near these margins, the basalt is typically ~5–10 m thick, so the altitude of any directly underlying gravel can be estimated roughly by subtraction. *Besançon and Sanlaville* [1981] and *Sanlaville* [2004] have depicted this plateau as underlain by more-or-less continuous gravel, assigned to their terrace QfIII, except at its southern margin (Figure 3b). The basalt seems to have originated from a neck (Hammet ash-Shamiyah Qulayb, reaching 376 m asl) in the northern part of the plateau (at about [EV 520 704]), from which it flowed outward in all directions. The NW Zalabiyeh Plateau, now separated from this neck by the river, is almost flush with, but slightly lower than, the surface of the NE Halabiyeh Plateau, suggesting that it may be capped by the same basalt, in which case the Euphrates at the time of this eruption lay well to the northeast of its present course at this point. The landscape morphology suggests that a smaller neck, reaching 350 m asl, is present near the

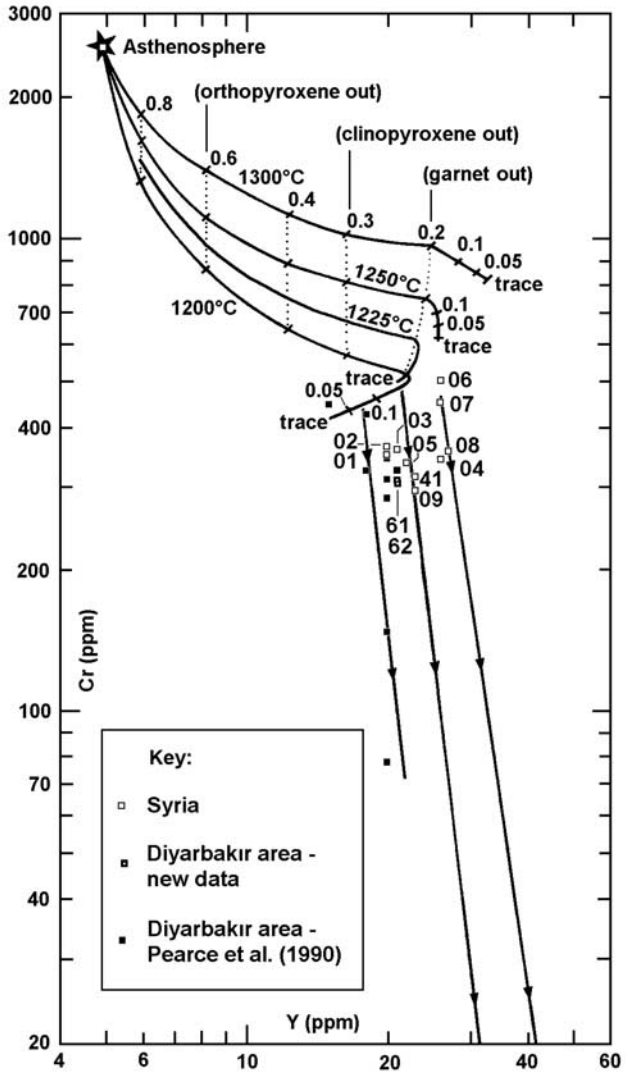


Figure 6. Cr versus Y diagram highlighting the roles of partial melting and fractional crystallization in the formation of the basalts in the study region. Solid lines are partial melting trends, calculated by *Pearce et al.* [1990] for garnet lherzolite (55% olivine, 20% orthopyroxene, 12.5% clinopyroxene, and 12.5% garnet) at 1200°C, 1250°C, and 1300°C, with each solid phase disappearing at the indicated degree of partial melting. See *Pearce et al.* [1990] for the values of the partition coefficients used and for sources of data. The line for 1225°C has been estimated by interpolation. Barbed lines indicate mafic crystallization trends, also from *Pearce et al.* [1990].

southern tip of the Halabiyeh Plateau (at about [EV 686 442]) and may have supplied some of the adjacent basalt.

[31] Basalt sample 03SY03 has yielded an Ar-Ar date of 2717 ± 20 ka (±2σ) (see section 3.2). Since this basalt flow unit caps the whole of the eastern margin of the Halabiyeh Plateau, it postdates all the gravels that lie beneath it, including those at much lower levels than at site 03SY03 itself. The gravels beneath the SE plateau margin, ~65 m above the present level of the Euphrates (Figure 9b; the Halabiyeh lower gravel in Figure 7), are thus no younger than ~2.7 Ma, whereas those beneath the NE plateau margin, ~110 m above the present river level (the Halabiyeh upper gravel in Figure 7), are even older.

[32] South of Halabiyeh, at Tibni (Figures 3b and 2b), gravel of terrace QfII is exposed along the right flank of the Euphrates valley [*Copeland*, 2004]. Borehole evidence [e.g., *Besançon and Sanlaville*, 1981; *Besançon and Geyer*, 2003] indicates that the base of this gravel is 27 m below the present river level, a value that seems fairly typical of the whole reach of the Euphrates between Raqqa and the border with Iraq; the maximum reported depth of the incision before the aggradation of this gravel is ~35 m below modern river level.

[33] For ~20 km between Madan and Shiha, the main road from Raqqa to Deir ez-Zor traverses the uplands to the west of the Halabiyeh Plateau (Figure 2a). For several hundred meters around the summit of this road, where it reaches ~305 m asl (~85 m above present river level), gravel is exposed in road cuttings, for instance at [EV 56806 52794] (site 4a in Figure 2b, illustrated in Figure 8h of *Demir et al.* [2007]) and at [EV 56988 52155] (site 4b). This ~5 m thick gravel, capped by a gypsum crust, displays fluvial sedimentary structures (e.g., cross bedding) and is unquestionably of Euphrates origin, given its polymict content. It has been grouped as part of terrace QfIII by *Besançon and Sanlaville* [1981] and *Sanlaville* [2004]. According to their mapping, this gravel coincides with a succession of upland flats that rise gradually toward the ESE, reaching ~320 m asl near the SW corner of the Halabiyeh Plateau (Figure 2b). However, the upper surface of the gravel at site 4a (~285 m asl) is ~20 m lower than that at site 4b, not in keeping with this trend, raising the possibility that multiple levels are present, rather than a single terrace deposit. The fluvial deposits at these two different levels are designated as the Madan upper and middle gravels in Figure 7. The area to the SW of the Raqqa to Deir ez-Zor road, ~4–5 km to the southwest, is formed in another succession of flats some ~25–30 m higher (Figure 2b). Much of this area was mapped by *Ponikarov and Mikhailov* [1964] as fluvial gravel of inferred "middle Pleistocene" age. However, this sequence of flats diverges downstream from the lower one, just as the lower one diverges downstream from the present river level (see section 3.2).

[34] The lower terraces in this area include *Besançon and Sanlaville*'s [1981] type locality for terrace QfI (locality 5 in Figure 2b; about [EV 669 536], near the NW corner of the Halabiyeh Plateau), the deposits of which they termed the "Abu Chahri Formation." *Copeland* [2004] reported "Levallois-like" artifacts from these deposits. According to *Besançon and Sanlaville* [1981], recent incision by the Abu Chahri tributary wadi has exposed ~15 m of Euphrates deposits, comprising gravel (base not seen) with a sandy matrix overlain by beige silt and reddish silt with some gravel clasts. *Besançon and Geyer* [2003] considered that these three superimposed units represent deposition in MIS 6,

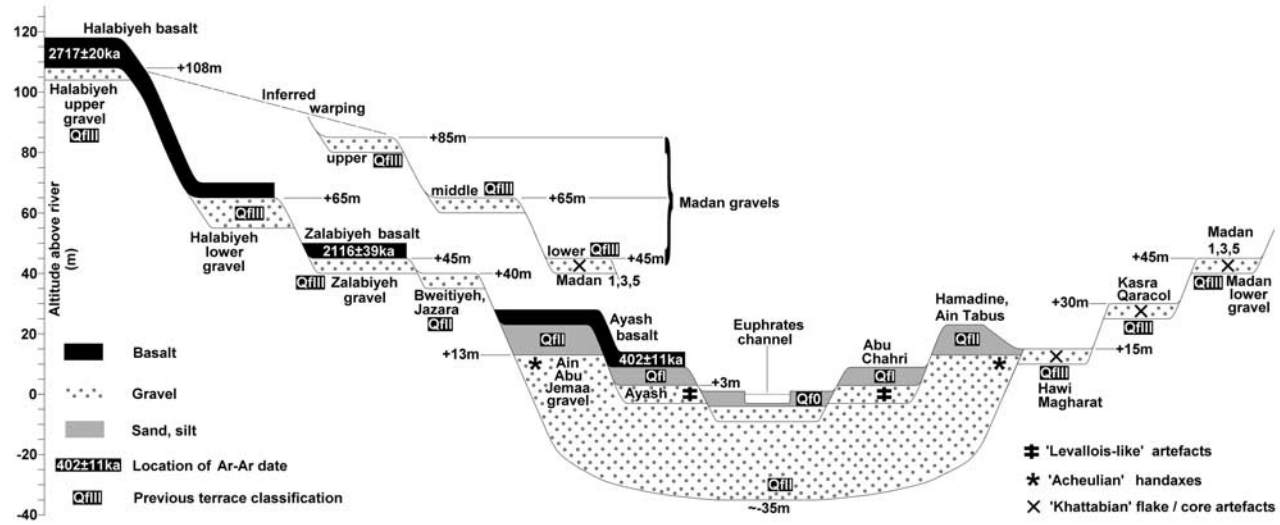


Figure 7. Schematic transverse profile, not to horizontal scale, illustrating the disposition of Euphrates terrace deposits at the sites discussed in the area between Madan and Deir ez-Zor. Sources of information are reported in the text; they include the Ar-Ar dating results in Figure 4. Bedrock is unshaded; Euphrates deposits above the level of the Halabiyeh upper gravel are omitted. The grouping of sites is schematic, with those that have yielded age control evidence on the left and those that have been reported [by *Copeland*, 2004] as yielding artifacts (see also Table 1 and discussion in the text) on the right. The warping inferred to have affected the Halabiyeh upper gravel is consistent with folding across the Jebel Bishri anticline axis [cf. *Litak et al.*, 1997]. Corresponding warping has not been resolved in any of the younger terrace deposits. See Figure 3 for site locations.

MIS 4, and MIS 2, respectively. According to *Sanlaville* [2004], these deposits are locally banked against older sediments, assigned to terrace QfII. The stratigraphic succession is thus very similar to that in the Ayash/Abu Jemaa area farther downstream (Figures 8a and 9a). By analogy, an age of MIS 12 can now be inferred for the deposits forming terrace QfI, those of terrace QfII being older.

[35] About 10 km farther upstream, artifacts have been reported in situ [e.g., *Copeland*, 2004] from much higher-level gravels exposed in quarries, ~2–3 km SE of the town of Madan adjoining the Wadi Khneifess (sites Madan 1, 3 and 5 in Figure 2b; also Figure 3). This gravel, which is banked against the bedrock forming the southern margin of the Euphrates valley, was assigned to terrace QfII by *Besançon and Sanlaville* [1981] but has since been reassigned to QfIII [e.g., *Copeland*, 2004] on the basis of the artifact assemblage, comprising deeply patinated flakes, cores, choppers and picks but no hand axes. Comparison of their mapped extent (Figure 3b) with the modern SRTM imagery (Figure 2b) indicates that the deposits forming this terrace reach ~265–270 m asl or ~45–50 m above the present level of the Euphrates. In Figure 7 these deposits are designated as the Madan lower gravel, to distinguish them from the older gravels at higher altitudes in the same area. The Ar-Ar date from basalt capping comparable gravel at Zalabiyeh, to be considered next (Figure 7), suggests an age of ~2 Ma for this gravel and any artifacts it contains.

4.3. Zalabiyeh Plateau and Its Surroundings

[36] For ~10 km between Jazara and Kibr, the Euphrates flows between the basalt-covered Halabiyeh and Zalabiyeh plateaus (Figure 3b). Along this reach its valley is much narrower than the >10 km width elsewhere, being <1 km wide, constrained by the erosion-resistant basalt that flanks it on both sides (Figures 2b and 8d). The ruined Zalabiyeh fortification overlooks this narrow Euphrates gorge from a promontory where basalt caps fluvial gravel. As schematically illustrated in Figure 9b, the basalt cascades partway down the margin of this SW corner of the ~100 km^2 Zalabiyeh Plateau toward present river level. However, the precise disposition of the basalt here is difficult to judge, as much of it has been quarried away.

[37] The Zalabiyeh basalt appears to have originated from a neck, Jebel Mu'ayzilah, ~5 km NNE of Kibr (at about [EV 800 505]), from which it flowed southwestward. *Besançon and Geyer* [2003] reported that at Zalabiyeh the surface of this basalt reaches 260 m asl, overlying fluvial gravel at 255 m asl, ~45 m above present river level (Figure 9b). *Besançon and Sanlaville* [1981] and *Sanlaville* [2004] have assigned this gravel to their terrace QfIII, to which they have attributed a "Mindel" or MIS 12 age. SRTM data (Figures 2b and auxiliary material) place the top of the basalt in this area slightly lower, at ~250–255 m asl.

[38] Sample 03SY05 was collected from ~1.5 m above the base of a ~5 m thick basalt exposure in an old quarry some 300 m NNE of Zalabiyeh ([EV 76896 48300]). At

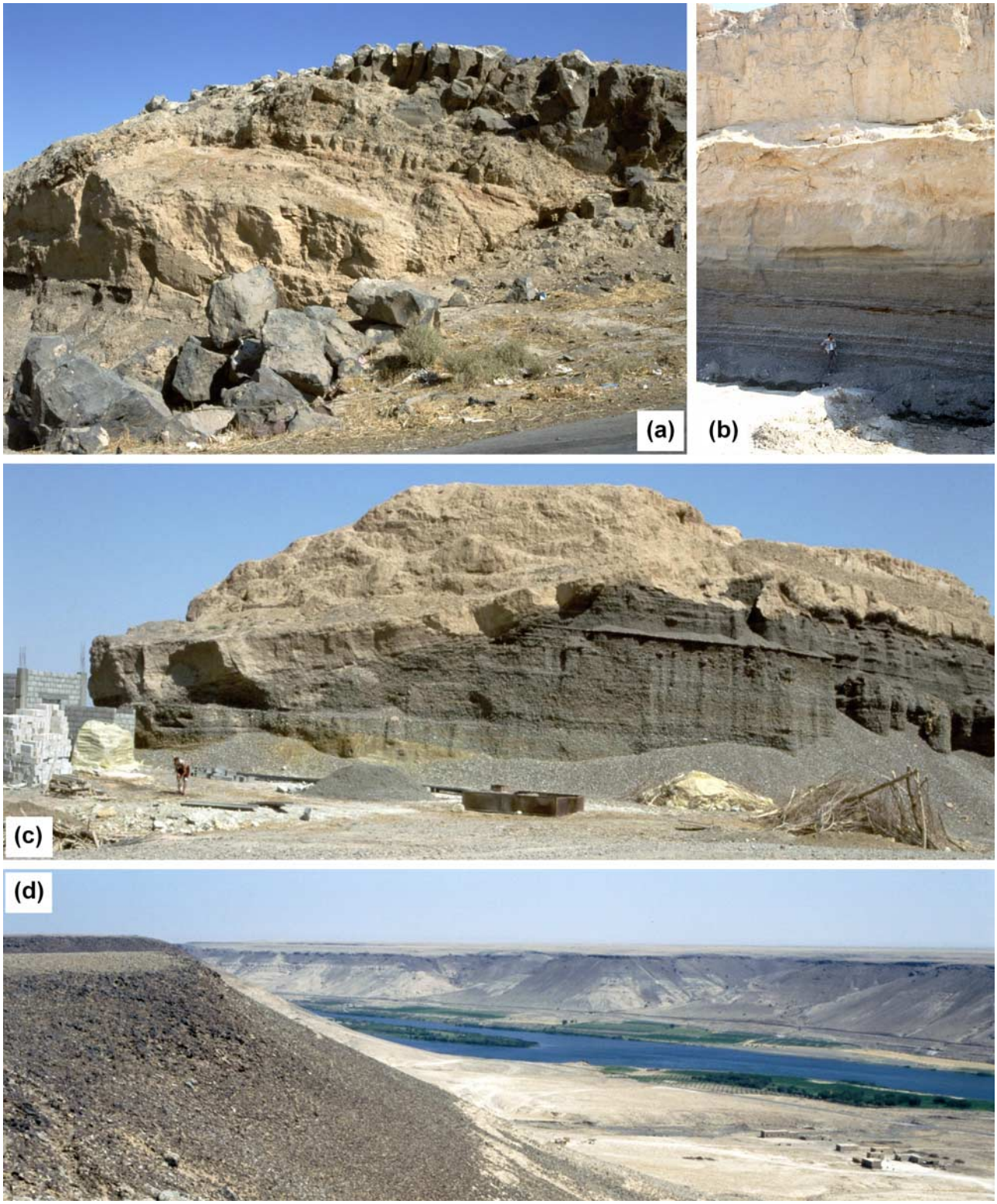


Figure 8

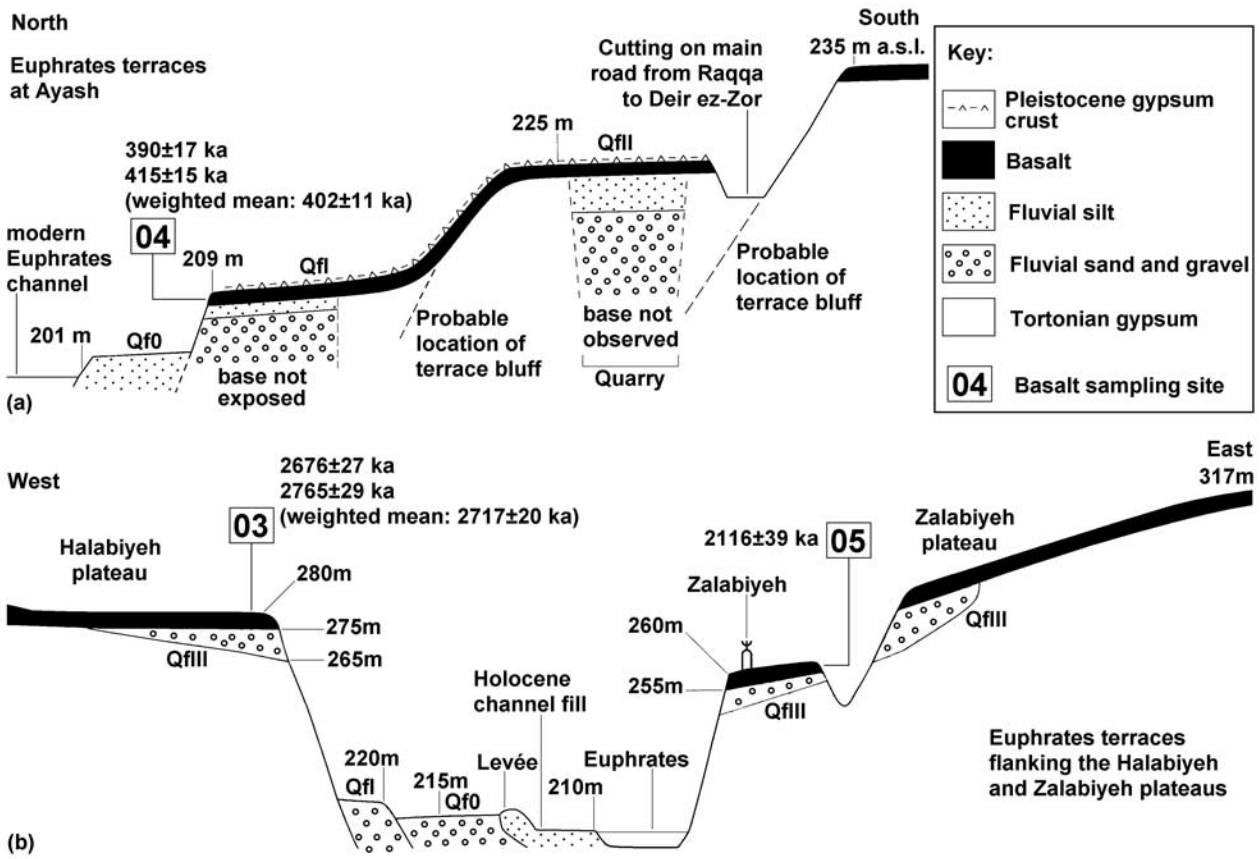


Figure 9. (a) Schematic cross section, not to horizontal scale, through the basalt flow and Euphrates terrace deposits at Ayash (illustrated in Figure 8a), showing the position of the sample site. Adapted from Figure 2 of *Westaway et al.* [2005a], based on Figure 12 of *Besançon and Geyer* [2003]. (b) Schematic cross section, not to horizontal scale, across the Euphrates gorge between the Halabiyeh and Zalabiyeh plateaus (illustrated in Figure 8d), showing dated sample sites. It is evident that the basalt flow sampled at Zalabiyeh cascades to a lower level within the Euphrates gorge than does that at Halabiyeh, consistent with its younger Ar-Ar age. The rise to 317 m represents the Jebel Mu'ayzilah neck, NNE of Kibr, from which the Zalabiyeh basalt erupted. Adapted from Figure 3 of *Westaway et al.* [2005a], based on Figure 11 of *Besançon and Geyer* [2003].

Figure 8. (a) View to the SSE looking at the bluff between Euphrates terraces Qf0 and QfI, exposed at [EV 94614 20938] in a small quarry at the tip of the Ayash basalt flow, where sample 03SY04 was collected (see Figure 1 or 3c for location). Dark Euphrates gravel (bottom left) is overlain by lighter colored silty sand, itself capped by basalt, as illustrated schematically in Figure 9a. (b) Quarry face in Euphrates terrace QfII, NW of Rasafeh at [EV 88189 25181]. About 5 m of well-stratified sand and gravel (base not exposed) is overlain by ~10 m of flood loam. The sand and gravel generally coarsen upward near the base of this exposed section, then fine upward, with complex interbedding of sand and loam at its top. The upper, relatively fine, part of this gravel displays clear cross bedding indicating paleoflow to the southeast. (c) Quarry face at [EV 79643 31827], in Tarif, exposing the uppermost ~5 m of Euphrates gravel, which has been channelized and then overlain by flood loam to make an additional thickness of ~3 m. These deposits were also grouped within terrace QfII by *Besançon and Sanlaville* [1981]. Note that the deposits illustrated in Figures 8b and 8c form the uppermost parts of very thick aggradations, the bases of which are up to ~35 m below present river level, as illustrated schematically in Figure 7. (d) View northward from [EV 73720 52122], near the point where sample 03SY03 was collected, looking upstream across the Euphrates gorge from the edge of the basalt-capped Halabiyeh Plateau toward the similar Zalabiyeh Plateau on the opposite side (see Figure 1, 2b, or 3b for location). Basalt talus obscures underlying fluvial gravel (of terrace QfIII) in this view, which is locally ~8 m thick. Terraces Qf0 and QfI can also be observed just above river level.

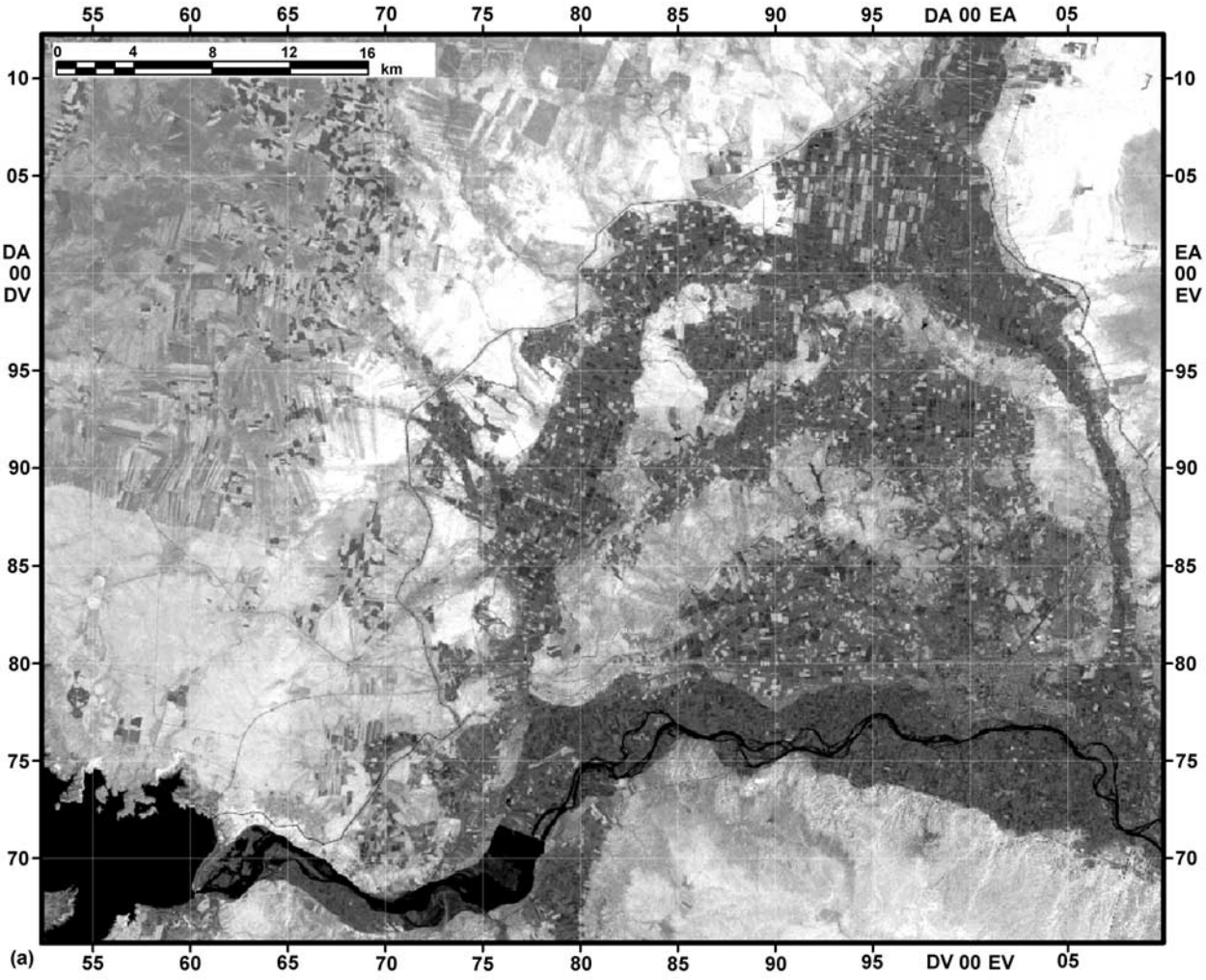


Figure 10a. Landsat ETM+ image of the Raqqa area, displayed using the same coordinate system and reference frame as Figure 2a showing localities discussed in the text.

points nearby, Euphrates gravel was observed banked against bedrock and overlain by this basalt. The SRTM data, located by GPS, indicate that the basalt surface is locally ~255 m asl, placing the top of the underlying gravel at ~250 m asl, ~40 m above the river. However, since both GPS measurements and the SRTM data might be adversely affected by the steep slopes and limited sky visibility at this plateau margin location, the altitude of the gravel (its top), ~45 m above present river level is taken from *Besançon and Geyer* [2003] (Figure 9b). The new date of 2116 ± 39 ka (Table 2 and Figure 4e) indicates that this fluvial gravel is significantly older than the middle Pleistocene age previously suggested.

[39] Just east of Jazara, on the left flank of the Euphrates valley north of the Zalabiyeh Plateau (Figure 2b), the upper surface of an extensive spread of Euphrates gravel is visible (around [EV 72070 59395], site 3 in Figure 2b), at ~245 m asl, ~35–40 m above the present river. Like its counterparts farther downstream, it has been grouped within terrace QfII [e.g., *Besançon and Sanlaville*, 1981; *Sanlaville*, 2004]. It can now be inferred that it is of roughly the same age as the gravel at Zalabiyeh, given that both gravels are at similar heights above the Euphrates (Figure 7).

[40] South of Zalabiyeh, between Kibr and Kasra, the left flank of the Euphrates valley is disrupted by an extensive meander scar, below which is an oxbow lake called Surat al-Kasra (Figure 2a). Downstream of this, widespread deposits of Euphrates gravel crop out, for instance in a quarry at site 1 in Figure 2b, (at [EV 83344 37146]); this site appears to be the locality called Kasra Qaracol by *Copeland* [2004]. The ~5 m of polymict gravel exposed at this site, clearly of Euphrates origin, is well stratified and well sorted, with clast sizes up to ~40 cm, and is overlain by ~1 m of loam. This gravel, like others in the area, was tentatively interpreted as middle Pleistocene by *Ponikarov and Mikhailov* [1964]. *Besançon and Sanlaville* [1981] and *Sanlaville* [2004]

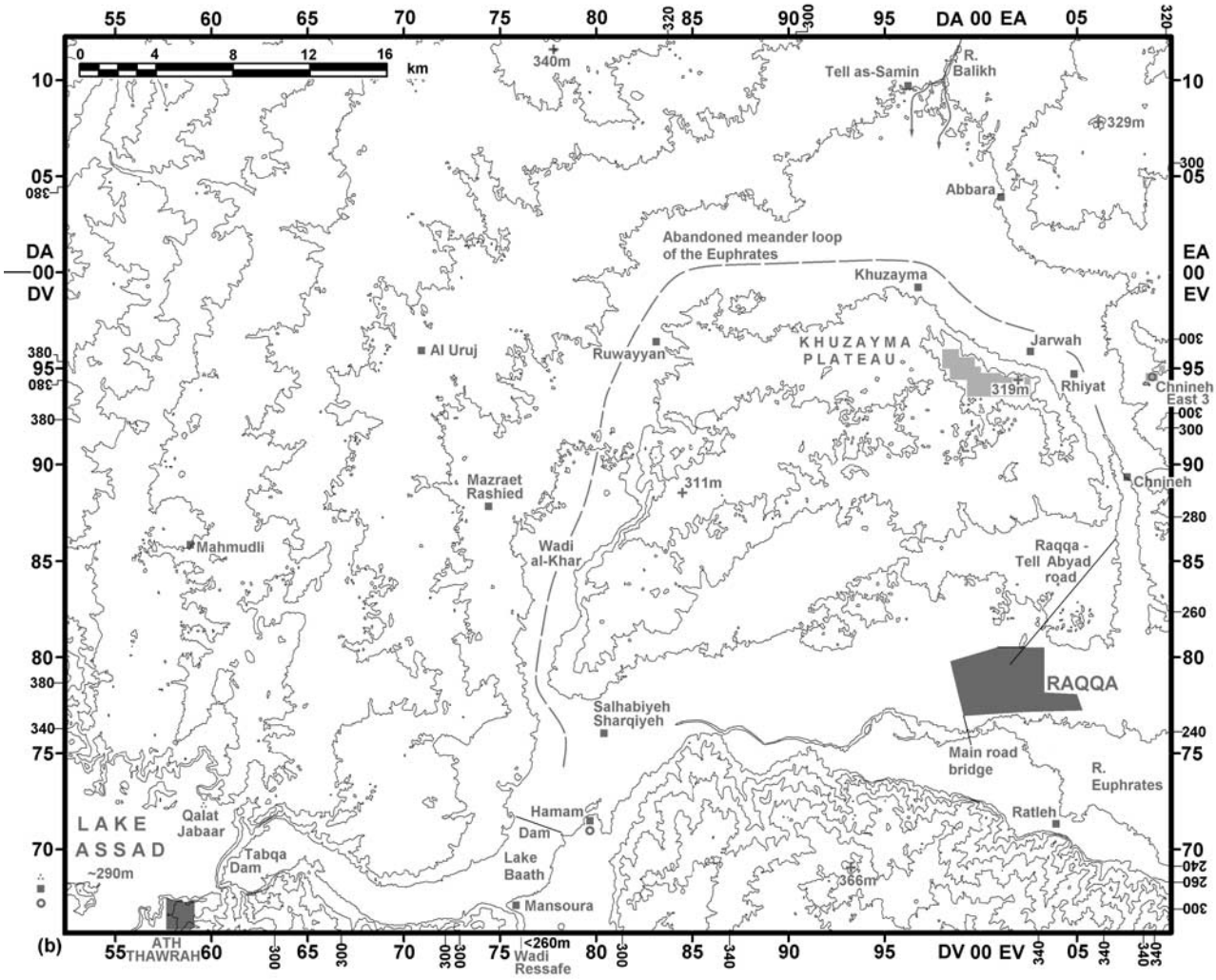


Figure 10b. Contour map with labeled 20 m contours derived from SRTM imagery. Specifications, coordinate system, and reference frame are as for Figure 2. Between [EV 03192 81657] and [EV 05978 84938], the main road from Raqqa to Tell Abyad (illustrated) climbs northeastward over a succession of flats, at altitudes (estimated using crude leveling, handheld GPS and SRTM imagery) of ~255, ~260, ~264, and ~266 m, or ~15–26 m above the present level of the Euphrates. There are no local road cuttings where exposures of gravel could be identified to provide confirmation of a fluvial origin of these landforms. This whole area has been assigned to terrace QfII by *Besançon and Sanlaville* [1981] (Figure 3a). However, the impression created is that the designated terrace QfII in this area is in reality a succession of individual terrace levels. See text for discussion. The auxiliary material includes another SRTM topographic image of this area, with 5 m contours.

designated it as part of their terrace QfII (Figure 3c). However, it is much higher relative to the present river than the type locality for this terrace (Figure 9a); from the SRTM imagery its upper surface height can be estimated as ~235–240 m asl (~30–35 m above the Euphrates). *Copeland* [2004] mentioned that deeply patinated flint artifacts had been recovered from this gravel, as well as quartz "choppers," and on the basis of their characteristics reclassified it as part of terrace QfIII, not QfII. Given its altitude (Figure 7), this gravel can tentatively be inferred to be somewhat younger than that at Zalabiyeh.

[41] On the right flank of the Euphrates valley, at Bweitiyeh (opposite Kasra), is a terrace flat, estimated from the SRTM imagery to rise to ~240–245 m asl (site 2 in Figure 2b; [EV 77391 36824]), ~35–40 m above present river level. Assigned to terrace QfII by *Besançon and Sanlaville* [1981], it was, like the gravel at Jazara, not later reclassified as QfIII [cf. *Sanlaville*, 2004], despite being at a similar height to other QfIII terrace deposits (Figure 7).

From the available SRTM heights for this and other key localities (discussed in sections 4.1 and 4.2 and earlier in this section), it is suggested that the sites hitherto grouped as QfIII in fact comprise a number of distinct deposits at different altitudes, as schematically illustrated in Figure 7. The variability in altitude of deposits assigned to terrace QfIII has been noted previously, by *Besançon and Geyer* [2003] and *Copeland* [2004], who attributed this to the differential erosion of what was originally a single aggradation. The records from other parts of the region [e.g., *Tyráček*, 1987; *Bridgland et al.*, 2007] instead indicate the occurrence of multiple aggradations at different levels, an interpretation that is favored here for this reach of the Euphrates. However, further work will be required to determine the precise relations of these various deposits.

4.4. Raqqa Area

[42] Jebel Mankar West and East are cinder cones, located in the left bank of the Euphrates, ~20 and ~30 km east of Raqqa near Karameh (Figure 1). Composed mainly of scoria, they rise to ~370 m asl, ~135 m above the river. Along the southern flank of these volcanoes, the feather edge of their scoria can be seen to blanket part of Euphrates terrace QfII of *Besançon and Sanlaville* [1981], indicating that the former postdates the latter (not shown in Figure 3a, which omits the blanket of scoria surrounding these cones). The very fresh appearance of this volcanism led *Ponikarov and Mikhailov* [1964] to estimate a late Pleistocene age. Samples 03SY06, 07 and 08 were collected from a quarry in the western flank of Jebel Mankar West (see Tables 2 and 3 for site locations). Sample 06 was of scoria, 07 was of massive basalt that was ex situ (collected from loose material, the only available source of massive basalt) and 08 was from in situ vesicular basalt. As already noted, these samples represent the most mafic volcanism documented anywhere in this region (Table 3). Sample 03SY08 yielded an Ar-Ar date of 72 ± 20 ka ($\pm 2\sigma$), confirming the late Pleistocene age of this volcanism, which is indeed the youngest to have been dated in the region (Figure 4f). However, the last fraction of argon released by the step heating of this sample indicated a far greater age, of 99.222 ± 1.011 Ma ($\pm 2\sigma$), presumably reflecting inherited argon within some mineral phase with a relatively high closure temperature (Figure 4g).

[43] For ~20 km north of Raqqa, the modern Balikh-Euphrates interfluve forms a gravel capped upland, which reaches its highest point, 319 m asl, about [EV 020 945], ~80 m above the local level of the Euphrates (Figures 10a and 10b). *Demir et al.* [2007] illustrated this gravel at a site ~3 km NW of this high point, overlooking the modern Balikh valley, where the gravel reaches ~315 m asl; quarries in this Khuzayma area typically expose ~5 m of gravel (illustrated in Figure 8g of *Demir et al.* [2007]). *Besançon and Sanlaville* [1981] named this expanse of gravel the "Balikh Upper Conglomerate." However, its polymict character and typical gray matrix indicate that it was deposited by the Euphrates, not the Balikh. *Besançon and Sanlaville* [1981] attributed this gravel to their terrace QfIV, although according to the modified scheme of *Besançon and Geyer* [2003] it would probably be attributable to QfV. *Besançon and Sanlaville* [1981] reported other polymict gravels along the lower Balikh east of this interfluve plateau, which they attributed to the Balikh. However, there are no significant gravels farther upstream in the Balikh, which in any case has a catchment that reaches no farther north than the vicinity of Şanlıurfa in southern Turkey (Figure 1) and so cannot have transported clasts of metamorphic lithologies derived from Anatolia, as seen in the Balikh Upper Conglomerate. Indeed, the topographic imagery of this area (Figure 10b) reveals an abandoned meander loop, of comparable dimensions to the modern Euphrates valley, extending around the western and northern margins of this plateau and leading into the present course of the lower Balikh. This is evidently a section of former Euphrates valley, the abandonment of which caused the extension of the Balikh to its modern confluence with the Euphrates east of Raqqa. The terraces formed of polymict gravel, flanking the modern lower Balikh, were presumably deposited by the Euphrates before this loop was abandoned and are thus unrelated to the modern Balikh. An example is the QfIII fluvial gravel on the left side of the modern lower Balikh valley at ~300 m asl (~60–65 m above the level of the Euphrates at Raqqa) at site Chnineh East 3 (Figure 10b). This site, from which a small number of highly patinated flake artifacts have been reported [e.g., *Copeland*, 2004], has been regarded as the "type locality" of terrace QfIII within Syria [e.g., *Besançon and Sanlaville*, 1981; *Sanlaville*, 2004]. The mapping by *Besançon and Sanlaville* [1981] indicates that terrace QfII is the oldest that follows the modern west-east course of the Euphrates, postdating the cutoff of the Khuzayma meander loop (Figure 3a). East of the lower Balikh, Euphrates terraces QfI and QfII are well exposed along the minor road from Raqqa to Mazaret Badr (Figure 3a). For instance, at [EV 11926 78008] this road climbs onto the higher of these terraces, where fluvial gravel and thin overlying loam are exposed, its top reaching ~365 m asl, ~30 m above the local level of the Euphrates.

[44] Another feature evident in Figures 10a and 10b is the overall change in morphology of the Euphrates valley around Raqqa. At the point where the Tabqah Dam is now located, and farther upstream, the valley is relatively narrow, but it broadens downstream such that around the Balikh confluence the Holocene floodplain is ~8 km wide. This valley broadening appears to correlate with the downstream onset of deep incision before the aggradation of terrace QfII, which boreholes show to have reached ~35 m below present river level in the Raqqa area [*Besançon and Sanlaville*, 1981] (Figure 7). Except for the reach between the Halabiyeh and Zalabiyeh plateaus, the Holocene floodplain of the Euphrates remains ~10 km wide downstream almost to the border with Iraq (see section 5.2).

4.5. Shireen Area

[45] At Shireen, ~30 km south of the Syria-Turkey border, the Euphrates flows along a narrow (<1 km wide) gorge, now flooded by the Tishreen Reservoir. Contrasting markedly with the wider (>10 km) parts of the valley farther downstream, the constriction of the valley here results from

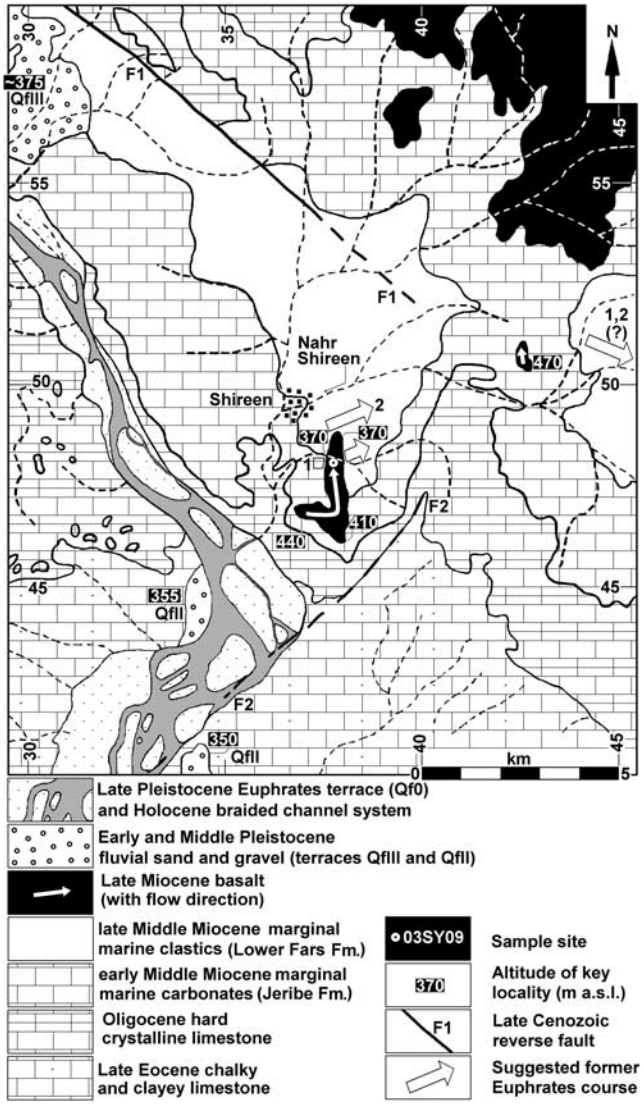


Figure 11. Geological map of the Shireen area (after *Ponikarov* [1966], adapted from Figure 9 of *Oguchi* [2001] with permission), showing the location of basalt sample 03SY09, located using the UTM coordinate system. The fluvial gravel underlying the basalt is not shown. The 1 denotes the inferred course of the Euphrates before the basalt eruption; 2 denotes its adjustment immediately afterward. In its natural state, the Euphrates was locally ~300 m asl; construction of the Tishreen Dam in the 1990s has impounded it at ~325 m.

relatively erosion-resistant Cenozoic marine limestone bedrock (Figure 11). In addition, there is no evidence of past incision along this reach to below the level of the modern valley floor, in contrast with the wider reach around and downstream of Raqqa (Figure 7). The local geological map shows several spreads of Euphrates gravel flanking this gorge (Figure 11). Two of these, on opposite flanks of the valley downstream of Shireen, reach ~355 m and ~350 m asl and have been assigned to terrace QfII [*Besançon and Sanlaville*, 1981]; they are ~45–50 m above the (flooded) valley floor. Another outcrop, at the gorge entrance in its left flank, appears highly dissected in the field and reaches ~370–375 m asl, ~20–25 m higher than the aforementioned QfII outliers and ~70 m above the valley floor, and was assigned to terrace QfIII by *Sanlaville* [2004].

[46] Basalt, previously inferred to be "early Pleistocene" [e.g., *Ponikarov and Mikhailov*, 1964], crops out widely in this region, capping the uplands that flank the valley (Figure 11). About 2 km SE of Shireen, in an old quarry (~370 m asl, at [DA 37571 47645]), the flow unit of picrobasalt that has now been dated (Table 2) overlies ~1 m thickness (base not exposed) of cemented, well-stratified and highly weathered gravel (Figures 12a and 12b). The basalt-gravel contact is subhorizontal, except at the south end of the exposure, where the basalt builds up from below a bluff at the edge of the gravel (Figure 12b). The ~3 m of basalt is likewise highly weathered; even its basal part, exposed in the quarry face, consists of core stones surrounded by rotten rock. Sample 03SY09 for Ar-Ar dating was collected from one such core stone.

[47] SRTM and Landsat imagery show that this basalt erupted from a neck at ~440 m asl, 1.6 km SSW of this site (Figure 11). It flowed initially east for 1 km before apparently becoming deflected northward along a local tributary valley, descending from ~400 to ~370 m asl in 1 km distance. However, the most distal ~1 km of this flow, within which the quarry site is located, is at a roughly constant level of ~370 m asl, implying that it caps a level surface, presumably on the Shireen gravel, although burying any preexisting fluvial terrace morphology, as is perhaps indicated by the above mentioned bluff (Figure 12b). The early Pleistocene age of this basalt seems to have been inferred [*Ponikarov et al.*, 1967] by analogy with the Pleistocene basalts in the nearby Karasu Valley [cf. *Yurtmen et al.*, 2002]. However, the degree of weathering is more characteristic of the late Miocene Homs basalt of western Syria (~6 Ma [*Mouty et al.*, 1992]) and the Karaçay basalt of SW Turkey (~7 Ma [*Westaway et al.*, 2005b]). Ar-Ar dating (Figure 4h and Table 2) has confirmed this, giving an age of 8809 ± 73 ka (±2σ), indicating a Miocene age for the underlying gravel.

[48] Interpretation of the Shireen gravel is hampered by its minimal exposure and weathered state. Abundant limestone and chert clasts were recognized, along with others too highly altered to be identified. It is likely that the chert originated in the ophiolite suite at the Neotethys suture, ~200 km to the north (Figure 1). The unidentifiable weathered clasts may well be igneous constituents of this ophiolite or metamorphic rocks from Anatolia, even farther north. The gravel would thus indicate the presence of an ancestral River Euphrates in this area at ~9 Ma. The disposition of the basalt and fluvial sediments suggests that the course of the Euphrates in the Shireen area was eastward rather than southward at this time, although the contemporaneous geometry of this river farther downstream has yet to be established (see Figure 1 and its caption).

[49] Gravels at Jaada, on the left flank of the Euphrates valley upstream of Shireen (Figure 1), assigned to terrace

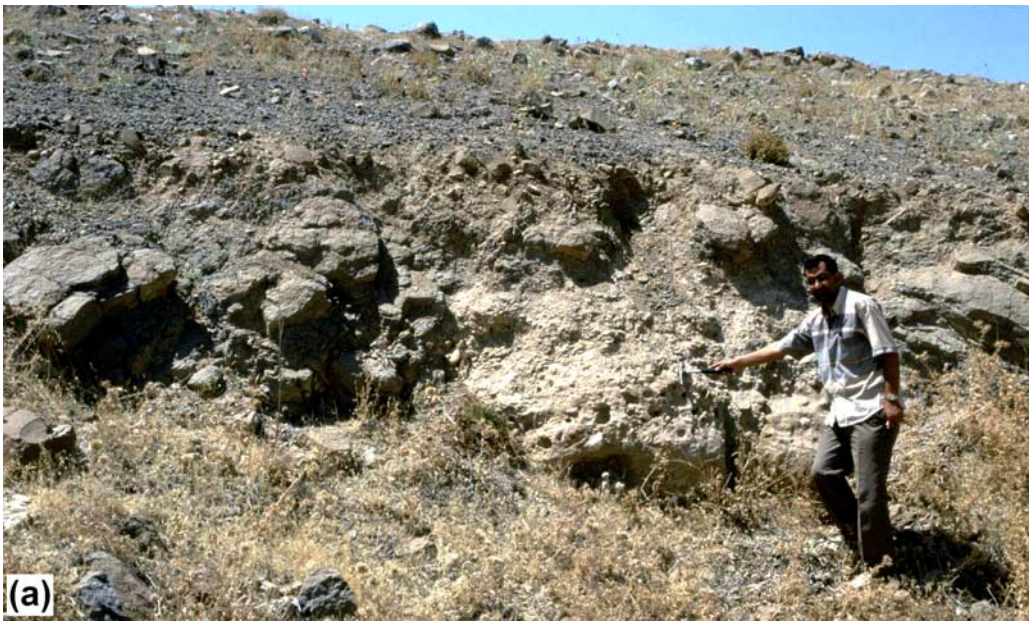


Figure 12a. Field photograph at [DA 37571 47645], looking west at the Shireen quarry exposure of gravel and overlying basalt.

QfII by *Sanlaville* [2004], reach ~345 m asl, for instance, at [DA 28131 59503], with up to 10 m thickness of overlying loam. Before it was dammed, the Euphrates here was ~305 m asl; thus the top of the gravel of terrace QfII is locally ~40 m above river level (Figure 12c). The reservoir level is ~325 m asl; it thus completely inundates the Holocene floodplain of the Euphrates in this area (Figure 12c), as well as the deposits assigned to terrace QfI. In this area, deposits assigned to terraces QfIV to QfI, belonging to the Euphrates and its right-bank tributaries, the Sajour (Sacır in Turkey) and Nizip (Figure 1), have yielded many Paleolithic artifacts [e.g., *Copeland*, 2004] (Table 1), although some of these sites have since been inundated by the Tishreen Reservoir. The pattern of reported artifact assemblages [cf. *Copeland*, 2004], with those from QfIV, QfIII and QfII in this area resembling those, respectively, from QfIII, QfII and QfI in the Raqqa–Deir ez-Zor area (see sections 4.1, 4.2, 4.3, and 4.4; Table 1), is consistent with much faster uplift along the former reach of the Euphrates than along the latter.

5. Discussion

5.1. Regional Synthesis of Volcanism

[50] Comparison of geological maps of the Shireen area [e.g., *Ponikarov and Mikhailov*, 1964; *Ponikarov*, 1966] and of adjacent parts of Turkey [e.g., *Ulu*, 1996a; *Terlemez et al.*, 1997] reveals that basalt flows considered equivalent in age to that at Shireen are contiguous, across the border, with the Yavuzeli Basalt of SE Turkey. *Ulu* [1996a] mentioned a K-Ar date of 10.6 ± 0.2 Ma for one of the Yavuzeli Basalt flow units east of Birecik but provided no supporting reference. *Terlemez et al.* [1997] cited an unpublished oil industry report in support of dating this volcanism to ~9–

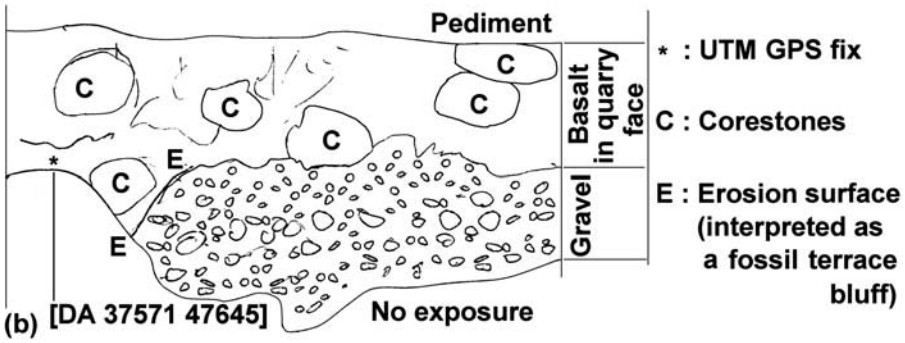


Figure 12b. Field sketch of the exposure in Figure 12a.

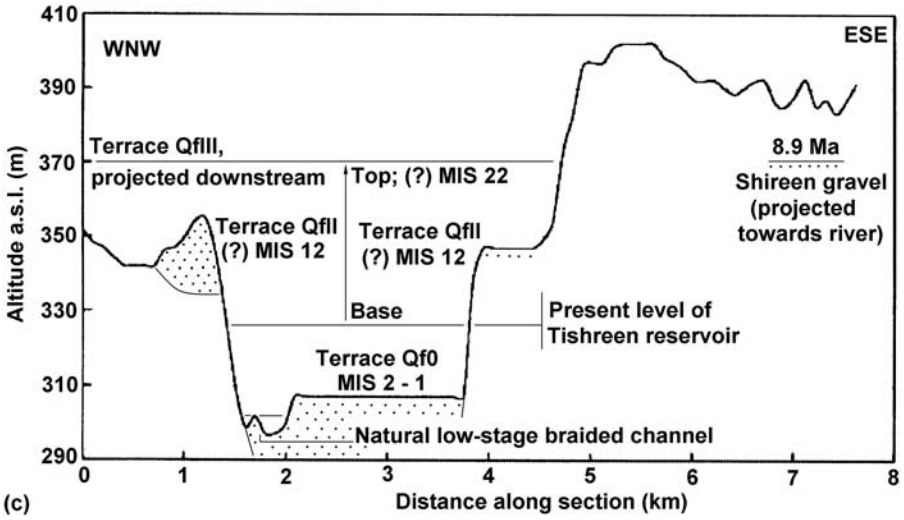


Figure 12c. Cross section through the Euphrates terrace staircase ~4 km south of this locality [after *Oguchi*, 2001, Figure 17] (with permission) (compare Table 4). See text for discussion. Heights of deposits illustrated correspond to the localities depicted in Figure 11.

8 Ma. The new date of 8.8 ± 0.1 Ma (Table 2) lies within the ~10.6–8 Ma age span of these earlier estimates. Recent mapping [e.g., *Ulu*, 1996b] recognizes the late Miocene Yavuzeli volcanism as distinct from the earlier middle Miocene eruptions in the same region and calls the latter the Çatboğazı volcanism. The only published isotopic dating of this earlier phase is provided by the five K-Ar dates in the range ~19–16 Ma by *Arger et al.* [2000] and *Tatar et al.* [2004], mentioned in section 1. Farther east, the voluminous Siverek Volcanics, which crop out widely northeast of Şanıurfa (Figure 1), have an age of 7.8 ± 1.7 Ma (±2σ), determined as the weighted mean of three K-Ar dates [*Bridgland et al.*, 2007], making them also broadly synchronous with the Shireen volcanism.

[51] For the later (post-3 Ma) phase of volcanism in northern Syria the most obvious comparison is with the Karacadağ volcanic field around Diyarbakır (Figure 1). The available age control for this Karacadağ volcanism has recently been reviewed, and supplemented with additional dating, by *Bridgland et al.* [2007]; K-Ar dates range from 2.7 ± 0.2 Ma to 101 ± 18 ka (both ±2σ). The overall age span of this Karacadağ volcanism is thus similar to that indicated by the new Ar-Ar dates (~2.7 Ma to ~70 ka; Table 2) from the Raqqa–Deir ez-Zor area. However, the preponderance of dating evidence indicates that a high proportion of the Karacadağ basalt erupted around 1.2 Ma [*Bridgland et al.*, 2007], a timing for which no counterpart has yet been identified in northern Syria.

[52] Following geochemical analysis, *Pearce et al.* [1990] reported the Karacadağ volcanism as alkali basaltic, the product of small-degree partial melting, with little or no crustal contamination, thus similar to the interpretation here of the contemporaneous volcanism in Syria. The principal difference is one of scale; one of the largest Plio-Pleistocene flow units in northern Syria, at Halabiyeh, covers ~100 km^2 (the whole of the Halabiyeh plateau surface in Figures 2a and 2b), with a typical thickness of ~5–10 m, indicating a volume of $\leq$1 km^3. In contrast, Karacadağ is a vast shield volcano, rising almost 2000 m asl, covering more than 3000 km^2 and with a volume of ~1000 km^3. To supplement the data from *Pearce et al.* [1990], Table 3 lists two new analyses of Karacadağ basalts from Diyarbakır (see also Figures 5 and 6). As Figure 6 indicates, unlike any of the Syrian samples, some Karacadağ basalts show evidence of significant crystal fractionation. The tendency for small-volume basaltic magmas to be relatively "primitive," whereas their larger-volume counterparts show significant fractional crystallization, has also been noted elsewhere [e.g., *Thompson et al.*, 1990].

5.2. Evolution of the Euphrates System

[53] As already noted, the development of the modern Euphrates system within the Arabian Platform relates to two main processes. The first is regional uplift, which has led to the net entrenchment of the Euphrates valley. The second is the progressive withdrawal of the sea from what are now the Arabian Platform uplands, also in response to the regional uplift, resulting in elongation of the river by well over 1000 km since the middle Miocene.

[54] In the limestone region upstream of Raqqa, the Euphrates valley is narrow and entrenched (see section 4.4; Figures 10a and 10b) before broadening out between Raqqa and the border with Iraq, except for the constricted basalt-capped reach at Halabiyeh (Figures 2a and 2b). Narrow valley morphology resumes ~15 km inside Iraq (about halfway between Anka and Anah; Figure 1). In between, the valley is typically much wider: >10 km wide between Raqqa and Deir ez-Zor and reaching a maximum width of

Table 4. Euphrates Terraces in the Shireen Area

Terrace[a]	Height,[b]	Description[b]	MIS	Age, ka	Rate,[c] mm yr^{-1}
Qf0 [Q3]	+8	fluvial sand/gravel	2	15	0.067
QfI [Q2][d]	+15–20	fluvial sand/gravel	6	140	0.057–0.093
QfII [Q1b][e]	+40–50	fluvial sand/gravel	12	430	0.077
QfIII[f]	+70	fluvial sand/gravel	22	870	0.072
QfIV[g]	+85	fluvial sand/gravel	68	1870	0.042
Shireen	+70	fluvial sand/gravel		8900	0.007
[Q1a]	+100	subaerial weathering	-	-	-

[a]Notation in brackets is after *Oguchi* [2001]. See the footnotes to Table 1 for a summary of the archaeology associated with each of terraces QfI to QfIV in this area. In most cases it is not clear whether the height quoted is for the top of fluvial gravel or the upper surface of the terrace.

[b]Data from *Oguchi* [2001] and *Sanlaville* [2004].

[c]Incision rates are calculated relative to 7 m above modern low-stage (autumn) predam river level; no ''channel lengthening correction'' has been applied. As an alternative, it is possible that the deposits forming terrace QfI may have aggraded in MIS 8 (~240 ka), which would indicate an incision rate of 0.033–0.054 mm yr^{-1}.

[d]The height of +20 m is for the upper surface of the terrace, from *Oguchi* [2001]; the height of +15 m is estimated from *Sanlaville* [2004]. The correlation of these deposits is our own proposal, since they were documented in different localities.

[e]The height of +40 m is for the top of fluvial gravel at Jaada, which *Sanlaville* [2004] assigned to terrace QfII, as discussed in the text. The height of +50 m is for the upper surface of the terrace, from Figures 11 and 12c.

[f]The height of +70 m is for the highest point within deposits that *Sanlaville* [2004] assigned to terrace QfIII, as illustrated in Figure 11.

[g]Terrace QfIV is not found in the Euphrates valley in this part of Syria. It has been found [e.g., *Sanlaville*, 2004] in the valley of the Sajour (Sacır in Turkey) right-bank tributary (which joins the Euphrates opposite Jaada; Figure 1). It has also been reported along the Euphrates itself around Birecik in the extreme south of Turkey [e.g., *Minzoni-Deroche and Sanlaville*, 1988]. Its reported height above local river level in the latter area is used here.

almost 20 km downstream of Deir ez-Zor around Mayadin (Figure 1). These variations in width may relate in part to differential susceptibility of bedrock lithologies to lateral erosion, the easily erodable clastic and evaporitic bedrock of the Upper Fars Formation coinciding with the wide valley downstream of Raqqa. In addition, as noted by *Besançon and Geyer* [2003], the Euphrates incised a wide valley to a depth of up to ~35 m below its present level before the aggradation of the deposits forming terrace QfII. The width of this reach of the modern Euphrates valley is in part a consequence of the width of the earlier incision. This phase of deep incision is not observed in other reaches of the Euphrates. Furthermore, as *Tyráček* [1987] noted, downstream from the end of the wide, previously incised reach in Iraq, the observed spacing of the terraces increases progressively. This is likely to reflect faster uplift, thus suggesting that the occurrence of deep incision before the aggradation of terrace QfII is related to relatively high local stability of the crust, an aspect that will be considered further during later uplift modeling (see section 5.3). By analogy, upstream altitudinal divergence of the Euphrates terraces, relative to the modern river, should also be expected in the vicinity of Raqqa. This is seemingly confirmed by the greater relative heights of each of the fluvial terraces around Raqqa in comparison with their counterparts around Halabiyeh and Deir ez-Zor (i.e., terrace QfII reaching ~30 m instead of ~20 m, and deposits of terrace QfIII with reported artifacts reaching ~65 m instead of ~45 m above present river level; see section 4.4).

[55] Evidence that this trend of increasing incision continues farther upstream is provided by the significantly greater altitude above present river level of the deposits assigned to terrace QfV in the Turkey-Syria border region than between Raqqa and Deir ez-Zor, ~200 m against ~110 m [*Minzoni-Deroche and Sanlaville*, 1988]. Table 4 thus suggests a tentative chronology for the Euphrates terrace deposits in the Shireen area. It is thus suggested that the deposits forming terraces QfI and Qf0 in this area aggraded during MIS 6 and 2, consistent with the interpretation of the adjacent Birecik area by *Kuzucuoğlu et al.* [2004]. For the older deposits, it is tentatively suggested that, in this area, terrace QfIII and not terrace QfII may mark MIS 22; if so, the incision since the gravel of this terrace was deposited has been ~70 m, much more than the 13 m observed at Ayash/Abu Jemaa (Figure 9a) but corresponding to the 70 m observed in the Tigris at Diyarbakır [*Bridgland et al.*, 2007], near the northern margin of the Arabian Platform. This difference, between the set of terrace ages inferred in the Manbij-Birecik and Raqqa–Deir ez-Zor areas is consistent with the different artifact assemblages, noted above (in sections 4.1, 4.2, 4.3, 4.4, and 4.5) that have been reported in the terraces in the two areas. Even if, instead, terrace QfII in the Shireen area marks MIS 22, then the incision since the end of gravel aggradation in this area has been significantly greater than at Ayash/Abu Jemaa (~40 m against 13 m; Table 4). The flooding of the Euphrates valley by the Lake Assad reservoir (Figure 1) prevents unambiguous correlation of the Euphrates terrace deposits between Shireen and the Raqqa–Deir ez-Zor area. To avoid further confusion resulting from the different sets of terrace ages evident in these two areas, it is suggested that the existing terrace symbols be modified to incorporate the reach of the Euphrates under discussion, introducing the letter M for the Manbij-Birecik area and R for the Raqqa–Deir ez-Zor area. Thus, for instance, terrace QfMIII can be correlated with terrace QfRII, both apparently representing fluvial aggradation in the late early Pleistocene.

[56] A final aspect of the regional geomorphology is the observation (Figure 1) that the modern Euphrates valley closely follows the southern margin of the former Upper Fars Formation depocenter; it does not flow axially along this former marine embayment. This suggests overall southward tilting of the landscape in this region since the late Miocene, which has deflected the river as far south as it can get without encroaching on the more erosion-resistant limestone uplands of central Syria. Previous workers [e.g., *Brew et al.*, 1997; *Litak et al.*, 1997; *Besançon and Geyer*, 2003] have suggested that the modern SE trending course of the Euphrates below Raqqa is in part structurally controlled, attributing this to local downwarping along the Euphrates Fault Zone. However, given the lack of evidence of active faulting oriented parallel to the NW-SE trend of the Euphrates between Raqqa and Deir ez-Zor, the above

mentioned mechanism of southward tilting, likely to be the result of a southward decrease in uplift rates, seems to be the main factor. It is supported by evidence for ~200 m of incision since the middle Pliocene by the River Tigris around Diyarbakır in SE Turkey [*Bridgland et al.*, 2007], whereas the Euphrates, ~250 km farther south, has achieved no more than ~110 m of net incision during the same interval, as indicated by the data presented here from the Halabiyeh Plateau and its surroundings (Figure 7).

[57] Overall, the late Cenozoic evolution of the Euphrates in the Arabian Platform can be summarized in four phases, as in Figure 1. Phase 1 marks the early middle Miocene when, as already noted, the ancestral Euphrates flowed into the Tethyan seaway. After incipient regional uplift created the north-south land bridge, roughly along the line Gaziantep-Aleppo, this ancestral drainage appears to have diverged, that to the west apparently forming the ancestral Ceyhan river system while that to the east flowed through the Shireen area and into the western end of the regressing Mesopotamian Basin (phase 2 in Figure 1, representing the late Miocene). Phase 3, representing the downstream channel lengthening in the Pliocene, is evidenced by the presence of clasts of Anatolian provenance in the high-level deposits of the Deir ez-Zor area (see sections 4.1, 4.2, and 4.3). Finally, the development of the modern Euphrates course upstream of the Turkish border (phase 4 in Figure 1) is no older than ~2 Ma, as determined from the ratio of the offset of its gorge through the EAFZ to the total slip on this fault zone [e.g., *Westaway*, 2004a].

5.3. History of Surface Uplift

[58] It was suggested in section 5.2 that differential regional uplift has manifested itself in the geomorphology of the Euphrates valley in Syria and Iraq. In addition to this regional tilting, it is clear that some of the older Euphrates terrace deposits have become warped as a result of anticlinal folding. The clearest evidence of this effect is west of the Halabiyeh Plateau (Figures 2b and 7), where some of the older deposits are back-tilted to the northwest, so as to tilt gently downward in the upstream direction (see section 4.2). This locality corresponds with the NW flank of the Jebel Bishri anticline (Figure 1), suggesting that the back-tilting results from the superimposition of local folding onto a background of regional uplift. Warping across the line of this anticline axis, shown schematically in Figure 7, is also evident in the seismic reflection record section in Figure 9 of *Litak et al.* [1997]. Another example is in the Shireen area (Figure 11), where the eastward Euphrates paleocourse inferred at the time of the local volcanism rises by ~100 m in ~5 km distance, in terms of the modern landscape. However, as Figure 11 indicates, this course transects two faults that have disrupted the late Cenozoic succession; slip on these will have also warped the landscape. There is thus no objection in principle to such a course, which would have led eastward and southward toward Raqqa (Figure 1), possibly controlled by a northwestward continuation of the "Euphrates Fault Zone" lineation that may also govern the course of the river between Raqqa and Deir ez-Zor [e.g., *Brew et al.*, 1997; *Litak et al.*, 1997; *Besançon and Geyer*, 2003]. At a later stage, processes in the Shireen area (including local faulting and folding, including NW down throw on fault F2; differential erosion; southward tilting; Figure 11) disrupted this course and deflected the river to form its modern valley upstream of Raqqa, which is now flooded by the Lake Assad reservoir (Figure 1).

[59] Although incision by the Euphrates can serve as a proxy for regional uplift (see section 3.4), it cannot be converted directly to uplift, because of the significant downstream lengthening as the coastline regressed. As already noted, it is probable that the middle Pliocene coastline followed the eastern margin of the modern Arabian Platform uplands, with the contemporaneous mouth of the ancestral Euphrates thus located somewhere near Khan al-Baghdadi (Figure 1). The Euphrates is at present ~70 m asl at this point [*Tyráček*, 1987], indicating that its incision since the middle Pliocene has been less than the accompanying regional uplift by the same amount, ~70 m. To allow for this effect, *Demir et al.* [2007] introduced a "channel lengthening correction," which was applied between the middle Pliocene and late early Pleistocene (i.e., between 3.1 and 0.9 Ma), when the coastline was considered to have shifted to approximately its present location. Like in other recent studies [e.g., *Westaway et al.*, 2002], it is assumed that the global ice volume was the same in the middle Pliocene as at present, consistent with the view that the East Antarctic ice sheet has been stable since then, as is generally accepted [e.g., *Denton et al.*, 1993; *Sugden et al.*, 1995]. It can thus be assumed that the global sea level was approximately the same in the middle Pliocene as at present. In many regions, uplift histories can be modeled in this manner as the response to two phases of LCFF, starting at 3.1 and 0.9 Ma, times that correspond to significant changes in global climate (e.g., *Westaway*, 2001, 2002b; *Westaway et al.*, 2004]. It is clear, however, that the vertical crustal motion revealed by the Euphrates deposits in the Raqqa–Deir ez-Zor region has been more complex than this, because it requires a switch from uplift to subsidence to explain the deep incision followed by the aggradation of the thick deposits forming terrace QfII, followed in turn by renewed uplift to explain the subsequent fluvial incision (Figure 13). Furthermore, to produce the observed reversals in the sense of vertical crustal motion, the uplift response to each phase of LCFF must start quickly, which requires the lower crustal layer to be thin, necessitating the choice of low W_i in all viable model runs, the optimum local value being 4.5 km.

[60] Figure 13 shows the preferred solution for the post-middle Pliocene uplift history represented by a composite data set for the Halabiyeh/Zalabiyeh/Tibni/Kasra/Ayash area (Figure 7). The uplift of this area is thus assumed to be regional, any contribution to the present terrace altitudes from local folding (see section 4.2) being neglected. This solution assumes four phases of LCFF, starting at 3.1, 2.0, 1.2 and 0.9 Ma, with the third of these phases having the opposite sign of ΔT_e to the others, to drive subsidence rather than uplift. This solution predicts that the observed deep incision in this area ended in MIS 36 and gravel of terrace QfII aggraded from then until MIS 22. The optimum

fit of the gravel forming the ~30 m level of terrace QfIII at Kasra is to MIS 68, and that of the ~110 m level of terrace QfIII beneath the Halabiyeh Plateau basalt is to the middle Pliocene at ~3.1 Ma, immediately prior to the initial phase of LCFF. The ~45–50 m gravel at Madan (Figure 2b), the Madan lower gravel in Figure 7, can be presumed to be of similar age to that at Zalabiyeh and thus to have aggraded just before the start of the 2.0 Ma phase of LCFF.

[61] No attempt has been made to model the regional uplift history before the middle Pliocene. Any such analysis would need to incorporate correction for the folding and faulting that affected this region at the time, as indicated, for instance, by the gentle upstream tilting of the oldest deposits west of the Halabiyeh Plateau (see section 4.2; Figure 2b). It is presumed that the gravel that reaches 320 m asl immediately west of this plateau, but is ~305 m asl near Madan, is the same age as the ~320 m asl Halabiyeh upper gravel beneath the basalt at the NE margin of the Halabiyeh Plateau (Figure 7), which has been assigned a nominal age of 3.1 Ma in the uplift modeling (Figure 13). The observed small component of tilting may indicate that part of the altitude of this gravel has developed as a result of local folding, not regional uplift; alternatively, this gravel may in reality predate the 3.7 Ma initiation of the present geometry of the DSFZ (Figure 1), when local folding may have ceased. More data are needed to distinguish between these alternatives and thus permit improved modeling of the effect of regional uplift in this locality. Second, any detailed prediction would also be entirely dependent on how the remaining ~140 m channel-lengthening correction (to adjust from sea level to the present 210 m asl level of the Euphrates at Halabiyeh) is assumed to be partitioned over time, which must at this stage be a matter of conjecture. However, it is evident from earlier discussion that the land surface in this area was probably close to sea level in the early late Miocene, ~11 Ma. If the gravels capping the Khuzayma Plateau north of Raqqa (Figure 10b) date from this time then there has been ~320 m of subsequent uplift; if the highest-level deposits SW of the Halabiyeh Plateau (Figure 2b) date from this time, then the figure is ~350 m. Since ~180 m of this is predicted to have occurred since ~3 Ma, the remainder, up to ~170 m, can be inferred to have occurred between ~11 and ~3 Ma, at a net time-averaged rate no greater than ~0.02 mm yr^{-1}.

[62] MIS 68 is widely recognized in NW Europe as a time of significant cold climate instability, associated with the Tiglian C4c cold stage that is recognized from pollen in the Netherlands and Germany [e.g., *Pross and Klotz*, 2002], and marked by gravel deposition in many rivers, an example being the gravel now forming the Stoke Row terrace of the River Thames in SE England [e.g., *Whiteman and Rose*, 1992; *Westaway*, 2002b; *Westaway et al.*, 2002]. The

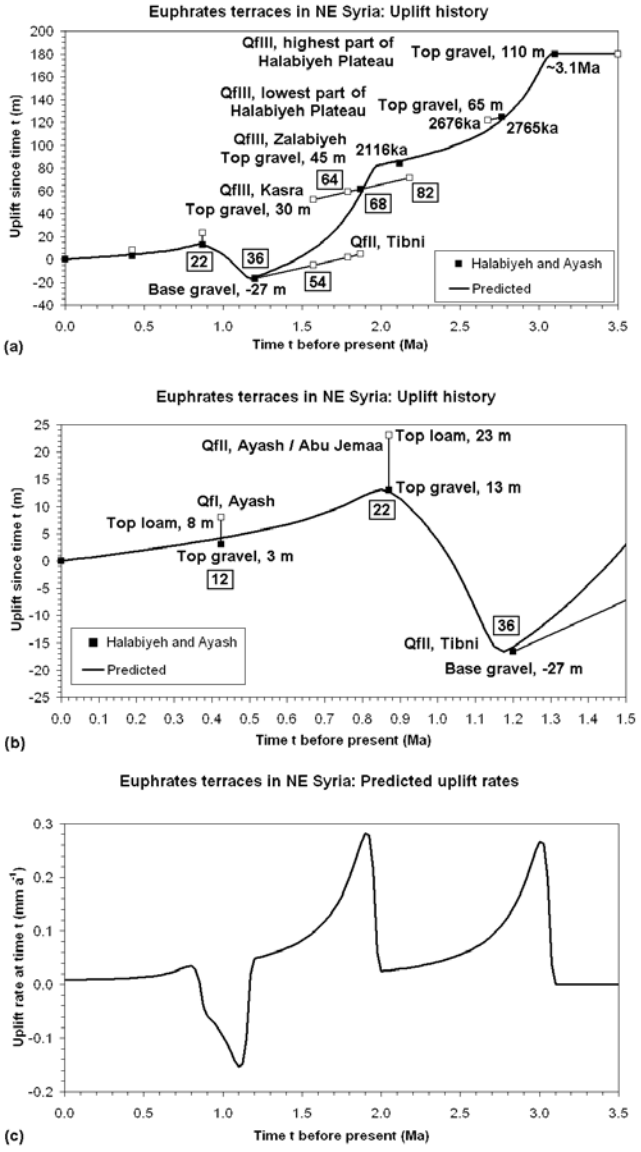


Figure 13. Modeling solution for the uplift history between Halabiyeh and Ayash. Terrace altitudes above the present river level (labeled) are as discussed in the text. Their altitudes are converted to estimates of uplift assuming a 70 m channel lengthening correction, which is applied at a uniform rate between 3.1 and 0.9 Ma, as discussed in the text. Model prediction, using the technique of *Westaway et al.* [2002], is based on the following parameter values: W_i = 4.5 km, u = 10°C km^{-1}, κ = 1.2 mm^2 s^{-1}, t_{o1} = 18 Ma, ΔT_{e1} = 0.1°C, t_{o2} = 3.1 Ma, ΔT_{e2} = −1.54°C, t_{o3} = 2.0 Ma, ΔT_{e3} = −1.50°C, t_{o4} = 1.2 Ma, ΔT_{e4} = +1.15°C, t_{o5} = 0.9 Ma and ΔT_{e5} = −0.41°C. This solution predicts net uplift by 13 m since 875 ka (MIS 22), 8 m since 950 ka (MIS 25), and 180 m since 3.1 Ma. Subsidence by 30 m, between relative levels of −17 and +13 m, is predicted to have occurred between 1175 and 850 ka. The maximum predicted uplift rates were 0.262 mm yr^{-1} around 3025 ka, 0.278 mm yr^{-1} around 1925 ka, and 0.034 mm yr^{-1} around 800 ka; the maximum predicted subsidence rate was 0.153 mm yr^{-1} around 1100 ka. (a) Uplift history. (b) Enlargement of the most recent part of Figure 13a. (c) History of variation of uplift rate.

suggestion that the ~30 m gravel of the Euphrates in NE Syria also dates from this time (Figure 13) raises the possibility that this climate instability also affected northern hemisphere latitudes much lower than those of NW Europe.

[63] The two oldest terraces recognized in NW Iraq by *Tyráček* [1987] (his terraces I and II) mark a broad paleovalley; deposits assigned to his terrace I crop out at ~230 m asl near the Syria-Iraq border and at ~150 m asl ~200 km farther downstream near the eastern margin of the Arabian Platform uplands, respectively ~60 m and ~80 m above present river level; terrace II is typically ~10 m lower. As noted in section 1, *Tyráček* [1987] suggested that the subsequent narrowing of the Euphrates valley in Iraq marked an increase in regional uplift rates, which he dated (by analogy with many river systems in Europe) to the late early Pleistocene (it would thus correspond with the 0.9 Ma phase of LCFF in Figure 13). However, applying the *Demir et al.* [2007] correlation scheme using the age constraints from the present study suggests instead that this change in valley morphology resulted from the 3.1 Ma phase of LCFF, which can now be seen (Figure 13) to be much more significant in this region. Nonetheless, *Tyráček* [1987] was correct to associate this change in valley morphology with an increase in regional uplift rates.

5.4. Wider Comparisons

[64] Similar dispositions of fluvial deposits to that in Figure 13, with abrupt variations in rates of vertical crustal motion and involving alternations between uplift and subsidence that largely cancelled over time and led to only limited net vertical crustal motion, have previously been reported elsewhere. They are observed across the East European Platform, for instance in the rivers Volga, Don, and Dnieper [e.g., *Matoshko et al.*, 2004]; in the Great Plains of the midcontinent United States, for instance in the lower reaches of the Platte River in eastern Nebraska, near its confluence with the Missouri [e.g., *Reed et al.*, 1965; *Bridgland and Westaway*, 2007]; and in the upper reaches of the Paraná river system in South America [e.g., *Bibus*, 1983; *Stevaux*, 1994]. In each of these cases, where dating evidence exists, the timings of the observed reversals in vertical crustal motions are similar to those in NE Syria (see section 5.3). As noted in section 5.3, this effect seems to be linked with a thin lower crustal layer, consistent with these regions being either within Early Proterozoic shield areas, with relatively low heat flow, or lying peripheral to Archaean cratons. In the core of an Archaean craton no mobile lower crustal layer is expected, leading to much greater crustal stability [cf. *Westaway et al.*, 2003], whereas in most regions of younger continental crust the mobile lower crustal layer is thicker and surface processes cause induced lower crustal flow responses that involve either continuous uplift or subsidence [e.g., *Westaway*, 2002b].

[65] The surface heat flow in the Arabian Platform is indeed low, being ~45 mW m^{-2} [e.g., *Medaris and Syada*, 1999; *al-Mishwat and Nasir*, 2004]. However, as previous workers [e.g., *Arger et al.*, 2000] have noted, this crust is much younger than in the other regions mentioned earlier in this section, being of Pan-African (i.e., latest Precambrian; ~600 Ma) age. Geobarometric, seismic, and gravity studies indicate that this crust is ~40 km thick [e.g., *Best et al.*, 1990; *Nasir and Safarjalani*, 2000] but is thought to include a layer of mafic underplating at least ~10 km thick [e.g., *Nasir and Safarjalani*, 2000; *al-Mishwat and Nasir*, 2004], which will not flow and thus forms the lower boundary to the overlying mobile layer [e.g., *Westaway*, 2001]. The presence of this mafic layer, in combination with the low heat flow, appears to be the main reason why the mobile lower crust is so thin in this region.

[66] In general, the thickness of the mobile lower crust in any region can be estimated as ~10 W_i/9 [e.g., *Westaway*, 1998]; from the uplift modeling above, it is thus ~5 km beneath NE Syria. It can thus be inferred that the local ~40 km thickness of crust typically consists of an upper brittle layer maybe ~25 km thick, with a ~5 km mobile layer and a ~10 km mafic basal layer. The resulting relatively low temperature at the base of this mobile layer will result in a relatively high effective viscosity for this layer; along with the thinness of this layer, this high viscosity will restrict rates of horizontal flow. The limited amounts of uplift in NE Syria since the middle Pliocene can thus be readily explained. As already noted, much more uplift has typically occurred on the same timescale within Anatolia, where the crust appears to lack mafic underplating and so its lower layer is typically thicker and hotter (and thus more mobile, i.e., less viscous) than in the interior of the Arabian Platform.

[67] Xenoliths from late Cenozoic basalts in southern Syria equilibrated under a much higher geothermal gradient than at present: ~90 mW m^{-2} or more [e.g., *Nasir and Safarjalani*, 2000]. It is thought that they date from around the time of the latest Precambrian (Neoproterozoic) consolidation of the crust of the Arabian Platform, at which time the thick layer of mafic underplating was emplaced, this magmatism possibly resulting from a mantle plume [e.g., *Nasir and Safarjalani*, 2000]. The lithosphere subsequently cooled to its present thermal state. The 99 Ma date of the last argon fraction released from Ar-Ar sample 03SY08 from Jebel Mankar West (Figure 4g) may well reflect the presence of a small proportion of such xenolith material, with inherited argon trapped in some high closure temperature mineral phase. Since none of the other samples exhibits similar behavior (Figure 4), there is no reason to think that any of the dates is affected by a systematic error originating from this source.

[68] Taking the base of the upper crustal brittle layer as marking the 350°C isotherm, as in previous studies, and assuming a 10°C km^{-1} geothermal gradient in the lower crust, as in Figure 13, a temperature of ~400°C can be tentatively estimated for the base of the mobile lower crustal layer and ~500°C at the Moho. Using the *Westaway* [1998] calibration, a temperature as low as ~400°C at the base of the mobile lower crust indicates an effective viscosity η_e for the lower crustal layer in excess of ~10^{22} Pa s. For comparison, in the Kula area of western Turkey, where the crust is ~30 km thick and the Moho temperature exceeds ~600°C, η_e has been estimated as no greater than ~10^{19} Pa s [*Westaway et al.*, 2004]. Even lower η_e can thus

be anticipated in eastern Anatolia, where the crust is thicker (see later in this section) and the Moho temperature can be expected to be significantly higher.

[69] The crustal thickness beneath eastern Anatolia is now tightly constrained at ~46 km from traveltimes of seismic waves [*Zor et al.*, 2003]. This crust is thus not much thicker than that beneath Arabia (~46 km against ~40 km) and yet high topography is present, ≥2 km above sea level, whereas most of Arabia is within ~500 m of sea level. As has been noted elsewhere [e.g., *Assumpção et al.*, 2002], the high density of the layer of mafic underplating beneath Arabia can be expected to load the crust, reducing the surface altitude. Nonetheless, the difference in altitude between Arabia and Anatolia has been seen as anomalous and has led to the recent development of ad hoc models for the late Cenozoic uplift of eastern Anatolia, in terms of the isostatic response to delamination of the underlying mantle lithosphere [e.g., *Şengör et al.*, 2003; *Keskin*, 2003], although this process is entirely hypothetical. Elsewhere, notably in Europe, modern explanations for late Cenozoic epeirogenic uplift, in terms of coupling between surface processes and induced lower crustal flow, have removed the need for this and other ad hoc explanations that were formerly prevalent [e.g., *Westaway*, 2001, 2002a, 2002b]. The same may well be true for eastern Anatolia: the much greater mobility of the lower crust beneath Anatolia than beneath Arabia, causing the lithosphere of Arabia to be by far the stronger of the two, is presumably the main reason why their Cenozoic continental collision has resulted in much greater deformation of the former than of the latter. It also explains how it is possible for the crust of eastern Anatolia, with much higher topography (~2–3 km), to coexist in isostatic equilibrium adjacent to Arabia: the lower crust of Arabia is so stiff that rates of outflow from beneath Anatolia are limited. This situation is thus a smaller-scale analogue of the continental collision between India and Eurasia, where the higher topography of Tibet than of India is dynamically maintained by the contrast in rheology between the Archaean craton of peninsular India and the much younger and hotter lithosphere of Tibet [e.g., *Westaway*, 1995]. This effect was also formerly explained as a consequence of delamination of the mantle lithosphere beneath Tibet [cf. *Molnar et al.*, 1993].

[70] *Pearce et al.* [1990] suggested that the Karacadağ volcanism (see section 5.1) was caused by decompression melting of the upper mantle, the result of crustal thinning due to extension. However, there is no independent evidence for extension in this region, nor is there any requirement for extension from regional kinematic models. In principle, a better explanation for Quaternary intraplate alkali basaltic volcanism, suggested previously for other parts of Turkey [e.g., *Arger et al.*, 2000; *Yurtmen et al.*, 2002; *Westaway et al.*, 2004] and other regions [e.g., *Westaway*, 2001], is that crustal thickening resulting from net inflow of lower crust has heated the mantle lithosphere, remelting volatile material that had previously frozen at depth. As previously suggested [e.g., *Arger et al.*, 2000], the original small-degree partial melting may have occurred progressively over time in the ancient geological past. As noted earlier, the preservation of inherited argon (since at least ~100 Ma) in the Jebel Mankar Ar-Ar dating sample (Figure 4g) is consistent with remobilization of material that had previously frozen in a relatively low-temperature environment, possibly within the layer of mafic underplating or the uppermost mantle lithosphere. However, the effect of reheating the lithosphere is difficult to calculate, not least because the crust and lithosphere are, in general, in a thermal nonsteady state due to the effect of surface processes causing induced lower crustal flow [e.g., *Westaway*, 2004b]. Although the depth of the base of the brittle layer is, in general, affected by rates of surface processes [e.g., *Westaway*, 2002c], to a first approximation it varies with crustal thickness. It can thus be expected to be a little deeper beneath Anatolia than beneath the Arabian Platform. The associated lateral pressure gradient can thus be expected to drive lower crust southward from Anatolia to Arabia. Since lower crustal flow, in general, is concentrated close to the Moho [e.g., *Westaway*, 1998], the material entering the Arabian crust is expected to be at a temperature somewhat in excess of 600°C, far hotter than the crust that is already present; it will thus have a dramatic heating effect on the crust directly below it, which will act to move any volatile material frozen in this layer closer to its solidus, potentially allowing remelting. The crustal thickening, resulting from this influx of material, will increase the lithostatic pressure in the underlying layer, which on its own would act to move the material away from its solidus, although in this region the temperature effect can be expected to be so dramatic that it will predominate. In qualitative terms, the basis thus exists for an explanation of the volcanism in this region in terms of this thermal effect of lower crustal flow, although formal calculations are beyond the scope of the present study and will be presented elsewhere.

6. Conclusions

[71] Ar-Ar dating of basalt flows capping terrace deposits of the River Euphrates in the Arabian Platform of NE Syria has enabled the development of a quantitative chronology for the late Cenozoic evolution of this important river system. This new chronology, supported by uplift modeling, indicates that most of the Euphrates deposits, and the associated incised landscape, are much older than has previously been thought. Since an initial increase in uplift rates around 3.1 Ma, incision rates by the Euphrates in NE Syria have varied dramatically over time; it is also estimated that between ~1.2 and ~0.9 Ma there was regional subsidence, resulting in fluvial aggradation. These abrupt variations in rates of vertical crustal motions, and reversals in their sense, are interpreted as consequences of the mobile lower crustal layer being relatively cold and thin, no more than ~5 km thick, due to the presence of a much thicker underlying layer of mafic underplating at the base of the crust. The surface uplift in this region is interpreted as a consequence of inflow of much hotter lower crustal material from beneath Anatolia, to the north. Release of melt, previously frozen in the mantle lithosphere or in the mafic underplated layer, by the heating effect of this inflow of

lower crust may explain the observed basaltic volcanism. The Ar-Ar dating indeed indicates that the Plio-Pleistocene phase of volcanism in this region began around 2.7 Ma, shortly after the increase in uplift rates at 3.1 Ma, a chronology shared with the much larger-scale Karacadağ alkali basaltic volcanism in the neighboring part of SE Turkey. In contrast to the fractionated Karacadağ alkali basalt, the contemporaneous small-volume flow units in NE Syria, which consist of basanite and foidite, are interpreted as primitive magmas with minimal crystal fractionation or crustal contamination. This study thus proposes an integrated, internally consistent explanation for this region's late Cenozoic volcanism and surface uplift.

[72] The generally greater ages implied for the Euphrates terraces and their contained artifacts have significant implications for the understanding of human occupation of this important region, which lies on the potential migration route out of Africa. This issue will be explored in future work.

[73] **Acknowledgments.** This work has been supported by HUBAK (Harran University Scientific Research Council), project 442 (T.D.). Support for field visits from the Council for British Research in the Levant is also gratefully acknowledged. We thank Keith Challis, Francisco Gomez, William Olszewski, and Andrew Shaw for helpful discussions and correspondence. We also thank Philip Collins and an anonymous reviewer for their thoughtful and constructive comments. This study contributes to IGCP 518 "Fluvial sequences as evidence for landscape and climatic evolution in the late Cenozoic" and to Focus 1 of the Fluvial Archives Group (FLAG).

References

Aktaş, G., and A. H. F. Robertson (1984), The Maden complex, SE Turkey: Evolution of a Neotethyan active margin, in *The Geological Evolution of the Eastern Mediterranean*, edited by J. E. Dixon and A. H. F. Robertson, *Geol. Soc. Spec. Publ.*, *17*, 375–402.

al-Mishwat, A. T., and S. J. Nasir (2004), Composition of the lower crust of the Arabian Plate: A xenolith perspective, *Lithos*, *72*, 45–72.

Alsharhan, A., and A. Nairn (1995), Tertiary of the Arabian Gulf: Sedimentology and hydrocarbon potential, *Palaeogeogr. Palaeoclimatol. Palaeoecol.*, *114*, 369–384.

Arger, J., J. Mitchell, and R. Westaway (2000), Neogene and Quaternary volcanism of south-eastern Turkey, in *Tectonics and Magmatism of Turkey and the Surrounding Area*, edited by E. Bozkurt, J. A. Winchester, and J. D. A. Piper, *Geol. Soc. Spec. Publ.*, *173*, 459–487.

Assumpção, M., D. James, and A. Snoke (2002), Crustal thicknesses in SE Brazilian Shield by receiver function analysis: Implications for isostatic compensation, *J. Geophys. Res.*, *107*(B1), 2006, doi:10.1029/2001JB000422.

Basaltic Volcanism Study Project (1981), *Basaltic Volcanism on the Terrestrial Planets*, 1263 pp., Elsevier, New York.

Besançon, J., and B. Geyer (2003), La géomorphologie de la basse vallée de l'Euphrate Syrien, in *La Basse Vallée de l'Euphrate Syrien du Néolithique a l'avenement de l'Islam*, vol. 1, edited by B. Geyer and J.-Y. Montchambert, pp. 7–59, Inst. Fr. du Proche Orient, Beirut, Lebanon.

Besançon, J., and P. Sanlaville (1981), Aperçu géomorphologique sur la vallée de l'Euphrate Syrien, *Paleorient*, *7*(2), 5–18.

Best, J. A., M. Barazangi, D. al-Saad, T. Sawaf, and A. Gebran (1990), Bouguer gravity trends and crustal structure of the Palmyride mountain belt and surrounding northern Arabian platform in Syria, *Geology*, *18*, 1235–1239.

Bibus, E. (1983), Reliefgenerationen am oberen Paraguai in Mato Grosso (Brasilien), *Z. Geomorphol., Suppl.*, *48*, 261–274.

Brew, G., R. Litak, D. Seber, M. Barazangi, T. Sawaf, and A. Al-Iman (1997), Basement depth and sedimentary velocity structure in the northern Arabian Platform, eastern Syria, *Geophys. J. Int.*, *128*, 617–631.

Bridgland, D. R. (2000), River terrace systems in northwest Europe: An archive of environmental change, uplift and early human occupation, *Quat. Sci. Rev.*, *19*, 1293–1303.

Bridgland, D. R., and R. Westaway (2007), Preservation patterns of late Cenozoic fluvial deposits and their implications: Results from IGCP 449, *Quat. Int*, in press.

Bridgland, D., G. Philip, R. Westaway, and M. White (2003), A long Quaternary terrace sequence in the valley of the River Orontes, near Homs, Syria, *Current Sci.*, *84*, 1080–1089.

Bridgland, D. R., P. Antoine, N. Limondin-Lozouet, J. I. Santisteban, R. Westaway, and M. J. White (2006), The Palaeolithic occupation of Europe as revealed by evidence from the rivers: Data from IGCP 449, *J. Quat. Sci.*, *21*, 437–455.

Bridgland, D., T. Demir, A. Seyrek, M. Pringle, R. Westaway, A. Beck, S. Yurtmen, and G. Rowbotham (2007), Dating Quaternary volcanism and incision by the River Tigris at Diyarbakır, SE Turkey, *J. Quat. Sci.*, *22*, 387–393.

Camp, V. E., and M. J. Roobol (1992), Upwelling asthenosphere beneath western Arabia and its regional implications, *J. Geophys. Res.*, *97*, 15,255–15,271.

Chaimov, T., M. Barazangi, D. Al-Saad, T. Sawaf, and A. Gebran (1990), Crustal shortening in the Palmyride fold belt, Syria, and implications for movement along the Dead Sea fault system, *Tectonics*, *9*, 1369–1386.

Collier, R. E. L., M. R. Leeder, M. Trout, G. Ferentinos, E. Lyberis, and G. Papatheodorou (2000), High sediment yields and cool, wet winters: Test of last glacial paleoclimates in the northern Mediterranean, *Geology*, *28*, 999–1002.

Copeland, L. (2004), The paleolithic of the Euphrates Valley in Syria, *Br. Archaeol. Rep., Int. Ser.*, *1263*, 19–114.

Coşkun, B., and S. Coşkun (2000), The Dead Sea Fault and related subsurface structures, Gaziantep Basin, SE Turkey, *Geol. Mag.*, *137*, 175–192.

Cox, K. G. (1980), A model for flood basalt volcanism, *J. Petrol.*, *21*, 629–650.

Demir, T., İ. Yeşilnacar, and R. Westaway (2004), River terrace sequences in Turkey: Sources of evidence for lateral variations in regional uplift, *Proc. Geol. Assoc.*, *115*, 289–311.

Demir, T., R. Westaway, D. R. Bridgland, A. Seyrek, and A. Beck (2007), Terrace staircases of the River Euphrates in southeast Turkey, northern Syria and western Iraq: Evidence for regional surface uplift, *Quat. Sci. Rev*, in press.

Denton, G. H., D. E. Sugden, D. R. Marchant, B. L. Hall, and T. L. Wilch (1993), East Antarctic ice sheet sensitivity to Pliocene climatic change from a dry valleys perspective, *Geogr. Ann.*, *75A*, 155–204.

Derman, A. (1999), Braided river deposits related to progressive Miocene surface uplift in Kahraman Maraş area, SE Turkey, *Geol. J.*, *34*, 159–174.

Fitton, J. G. (1987), The Cameroon line, West Africa: A comparison between oceanic and continental alkaline volcanism, in *Alkaline Igneous Rocks*, edited by J. G. Fitton and B. G. J. Upton, *Geol. Soc. Spec. Publ.*, *30*, 273–291.

Floyd, P. A., and P. R. Castillo (1992), Geochemistry and petrogenesis of Jurassic ocean crust basalts, ODP Leg 129, Site 801, *Proc. Ocean Drill. Program Sci. Results*, *129*, 361–388.

Gomez, F., M. Khawlie, C. Tabet, A. N. Darkal, K. Khair, and M. Barazangi (2006), Late Cenozoic uplift along the northern Dead Sea transform in Syria and Lebanon, *Earth Planet. Sci. Lett.*, *241*, 913–931.

Harford, C. L., M. S. Pringle, R. S. J. Sparks, and S. R. Young (2002), The volcanic evolution of Montserrat using $^{40}Ar/^{39}Ar$ geochronology, in *The eruption of the Soufrière Hills volcano, Montserrat, From 1995 to 1999*, edited by T. H. Druitt and B. P. Kojkelaar, *Mem. Geol. Soc. London*, *21*, 93–113.

James, G., and J. Wynd (1965), Stratigraphic nomenclature of Iranian Oil Consortium Agreement Area, *Am. Assoc. Pet. Geol. Bull.*, *49*, 2182–2245.

Jet Propulsion Laboratory (1998), Shuttle Radar Topographic Mission: Mapping the world in three dimensions, *JPL Rep. 400-713 7/98*, Calif. Inst. of Technol., Pasadena.

Johnson, R. W., J. Knutson, and S. R. Taylor (1989), *Intraplate Volcanism in Eastern Australia and New Zealand*, 408 pp., Cambridge Univ. Press, New York.

Karig, D., and H. Kozlu (1990), Late Palaeogene-Neogene evolution of the triple junction near Maraş, south-central Turkey, *J. Geol. Soc. London*, *147*, 1023–1034.

Keskin, M. (2003), Magma generation by slab steepening and breakoff beneath a subduction-accretion complex: An alternative model for collision-related volcanism in Eastern Anatolia, Turkey, *Geophys. Res. Lett.*, *30*(24), 8046, doi:10.1029/2003GL018019.

Kiden, P., and T. E. Törnqvist (1998), Can river terrace flights be used to quantify Quaternary tectonic uplift rates?, *J. Quat. Sci.*, *13*, 573–574.

Kukla, G. J. (1978), The classical European glacial stages: Correlation with deep-sea sediments, *Trans. Nebr. Acad. Sci.*, *6*, 57–93.

Kuzucuoğlu, C., M. Fontugne, and D. Mouralis (2004), Holocene terraces in the middle Euphrates valley between Halfeti and Karkemish (Gaziantep, Turkey), *Quaternaire*, *15*, 195–206.

Le Bas, M. J., R. W. Le Maitre, A. Streckeisen, and B. Zanettin (1986), A chemical classification of volcanic rocks based on the total alkali-silica diagram, *J. Petrol.*, *27*, 745–750.

Litak, R. K., M. Barazangi, W. Beauchamp, D. Seber, G. Brew, T. Sawaf, and W. Al-Youssef (1997), Mesozoic-Cenozoic evolution of the intraplate Euphrates fault system, Syria: Implications for regional tectonics, *J. Geol. Soc. London*, *154*, 653–666.

Lovelock, P. (1984), A review of the tectonics of the Middle East region, *Geol. Mag.*, *121*, 577–587.

Macklin, M. G., I. C. Fuller, J. Lewin, G. S. Maas, D. G. Passmore, J. Rose, J. C. Woodward, S. Black, R. H. B. Hamlin, and J. S. Rowan (2002), Correlation of fluvial sequences in the Mediterranean basin over the last 200 ka and their relationship to climate change, *Quat. Sci. Rev.*, *21*, 1633–1641.

Maddy, D. (1997), Uplift-driven valley incision and river terrace formation in southern England, *J. Quat. Sci.*, *12*, 539–545.

Matoshko, A., P. Gozhik, and G. Danukalova (2004), Key late Cenozoic fluvial archives of eastern Europe: The Dniester, Dnieper, Don and Volga, *Proc. Geol. Assoc.*, *115*, 141–173.

McClusky, S., et al. (2000), Global Positioning System constraints on plate kinematics and dynamics in the eastern Mediterranean and Caucasus, *J. Geophys. Res.*, *105*, 5695–5719.

Medaris, L. G., Jr., and G. Syada (1999), Pyroxenite xenoliths from Al Ashaer Volcano, Syria: Constraints on the thermal state of the subcontinental Arabian lithosphere, *Int. Geol. Rev.*, *41*, 895–905.

Middlemost, E. A. K. (1985), *Magmas and Magmatic Rocks: An Introduction to Igneous Petrology*, 266 pp., Longman's, London.

Middlemost, E. A. K. (1989), Iron oxidation ratios, norms, and the classification of volcanic rocks, *Chem. Geol.*, *77*, 19–26.

Miliaresis, G., and C. Paraschou (2005), Vertical accuracy of the SRTM DTED level 1 of Crete, *Int. J. Appl. Earth Obs. Geoinf.*, *7*, 49–59.

Minzoni-Deroche, A., and P. Sanlaville (1988), Le Paléolithique Inférieur de la région de Gaziantep, *Paleorient*, *14*, 87–98.

Molnar, P., P. England, and J. Martinod (1993), Mantle dynamics, the uplift of the Tibetan Plateau, and the Indian monsoon, *Rev. Geophys.*, *31*, 357–396.

Mouty, M., M. Delaloye, D. Fontignie, O. Piskin, and J.-J. Wagner (1992), The volcanic activity in Syria and Lebanon between Jurassic and actual, *Schweiz. Mineral. Petrogr. Mitt.*, *72*, 91–105.

Nasir, S., and A. Safarjalani (2000), Lithospheric petrology beneath the northern part of the Arabian Plate in Syria: Evidence from xenoliths in alkali basalts, *J. Afr. Earth Sci.*, *30*, 149–168.

Oguchi, T. (2001), Geomorphological and environmental settings of Tell Kosak Shamali, Syria, in *Tell Kosak Shamali, the Archaeological Investigations on the Upper Euphrates, Syria*, vol. 1, edited by N. Nishiaki and T. Matsutani, pp. 19–40, Oxbow, Oxford, U. K.

Pearce, J. A., J. F. Bender, S. E. De Long, W. S. F. Kidd, P. J. Low, Y. Güner, F. Şaroğlu, Y. Yılmaz, S. Moorbath, and J. G. Mitchell (1990), Genesis of collision volcanism in eastern Anatolia, Turkey, *J. Volcanol. Geotherm. Res.*, *44*, 189–229.

Perves, M. (1964), Préhistoire de la région du Moyen Euphrates, *Bull. Soc. Prehist. Fr.*, *61*, 422–435.

Ponikarov, V. (1966), Geological map of the Jarablus (J-37–III) quadrangle, 1:200,000 scale, Technoexport, Moscow.

Ponikarov, V., and I. Mikhailov (1964), Geological map of Syria, 1:1,000,000 scale, Technoexport, Moscow.

Ponikarov, V., et al. (1967), The geology of Syria: Explanatory notes on the geological map of Syria, scale 1:500,000. part I: Stratigraphy, igneous rocks, and tectonics, Technoexport, Moscow.

Pross, J., and S. Klotz (2002), Palaeotemperature calculations from the Praetiglian/Tiglian (Plio-Pleistocene) pollen record of Lieth, northern Germany; implications for the climatic evolution of NW Europe, *Global Planet. Change*, *34*, 253–267.

Rabus, B., M. Eineder, A. Roth, and R. Bamler (2003), The shuttle radar topography mission: A new class of digital elevation models acquired by spaceborne radar, *ISPRS J. Photogramm. Remote Sens.*, *57*, 241–262.

Reed, E. C., V. H. Dreeszen, C. K. Bayne, and C. B. Schultz (1965), The Pleistocene in Nebraska and northern Kansas, in *The Quaternary of the United States*, edited by H. E. Wright Jr. and D. G. Frey, pp. 187–202, Princeton Univ. Press, Princeton, N. J.

Renne, P. R., C. C. Swisher, A. L. Deino, D. B. Karner, T. L. Owens, and D. J. DePaolo (1998), Intercalibration of standards, absolute ages and uncertainties in $^{40}Ar/^{39}Ar$ dating, *Chem. Geol.*, *145*, 117–152.

Rigo de Righi, M., and A. Cortesini (1964), Gravity tectonics in Foothills Structure Belt of southeast Turkey, *Am. Assoc. Pet. Geol. Bull.*, *48*, 1911–1937.

Rose, J., X. Meng, and C. Watson (1999), Palaeoclimate and palaeoenvironmental responses in the western Mediterranean over the last 140 ka: Evidence from Mallorca, Spain, *J. Geol. Soc. London*, *156*, 435–448.

Sanlaville, P. (2004), Les terraces Pléistocènes de la vallée de l'Euphrate en Syrie et dans l'extrême sud de la Turquie, *Br. Archaeol. Rep., Int. Ser.*, *1263*, 115–133.

Şengör, A. M. C., S. Özeren, T. Genç, and E. Zor (2003), East Anatolian high plateau as a mantle-supported, north-south shortened domal structure, *Geophys. Res. Lett.*, *30*(24), 8045, doi:10.1029/2003GL017858.

Singer, B. S., and M. S. Pringle (1996), Age and duration of the Matuyama-Brunhes geomagnetic polarity reversal from $^{40}Ar/^{39}Ar$ incremental heating analysis of lavas, *Earth Planet. Sci. Lett.*, *139*, 47–61.

Steiger, R. H., and E. Jäger (1977), Convention on the use of decay constants in geo- and cosmochronology, *Earth Planet. Sci. Lett.*, *36*, 359–363.

Stevaux, J. C. (1994), The upper Paraná River (Brazil): Geomorphology, sedimentology and paleoclimatology, *Quat. Int.*, *21*, 143–161.

Sugden, D. E., D. R. Marchant, N. Potter Jr., R. A. Souchez, G. H. Denton, C. C. Swisher III, and J.-L. Tison (1995), Preservation of Miocene glacier ice in East Antarctica, *Nature*, *376*, 412–414.

Tatar, O., J. D. A. Piper, H. Gürsoy, A. Heimann, and F. Koçbulut (2004), Neotectonic deformation in the transition zone between the Dead Sea Transform and the East Anatolian Fault Zone, southern Turkey: A palaeomagnetic study of the Karasu Rift volcanism, *Tectonophysics*, *385*, 17–43.

Terlemez, H. Ç. İ., K. Şentürk, M. Sümengen, and A. Oral (1997), Geological map of the Antakya–L24 quadrangle, 1:100,000 scale, and accompanying 11 page explanatory booklet, Gen. Dir. of Miner. Res. and Explor., Ankara.

Thompson, R. N., P. T. Leat, A. P. Dickin, M. A. Morrison, G. L. Hendry, and S. A. Gibson (1990), Strongly potassic mafic magmas from lithospheric mantle sources during continental extension and heating; evidence from Miocene minettes of northwest Colorado, U.S.A., *Earth Planet. Sci. Lett.*, *98*, 139–153.

Tyráček, J. (1987), Terraces of the Euphrates River, *Sb. Geol. Ved Antropozoikum*, *18*, 185–202.

Ulu, Ü. (1996a), Geological map of the Suruç–L25 quadrangle, 1:100,000 scale, and accompanying 9 page explanatory booklet, Gen. Dir. of Miner. Res. and Explor., Ankara.

Ulu, Ü. (1996b), Geological map of the Urfa–K25 quadrangle, 1:100,000 scale, and accompanying 11 page explanatory booklet, Gen. Dir. of Miner. Res. and Explor., Ankara.

Weaver, B. L., D. A. Wood, J. Tarney, and J. L. Joron (1987), Geochemistry of ocean island basalts from the South Atlantic: Ascension, Bouvet, St. Helena, Gough and Tristan da Cunha, in *Alkaline Igneous Rocks*, edited by J. G. Fitton and B. G. J. Upton, *Geol. Soc. Spec. Publ.*, *30*, 253–267.

Westaway, R. (1995), Crustal volume balance during the India-Eurasia collision and altitude of the Tibetan Plateau: A working hypothesis, *J. Geophys. Res.*, *100*, 15,173–15,194.

Westaway, R. (1998), Dependence of active normal fault dips on lower-crustal flow regimes, *J. Geol. Soc. London*, *155*, 233–253.

Westaway, R. (2001), Flow in the lower continental crust as a mechanism for the Quaternary uplift of the Rhenish Massif, north-west Europe, in *River Basin Sediment Systems: Archives of Environmental Change*, edited by D. Maddy, M. Macklin, and J. Woodward, pp. 87–167, A. A. Balkema, Brookfield, Vt.

Westaway, R. (2002a), Geomorphological consequences of weak lower continental crust, and its significance for studies of uplift, landscape evolution, and the interpretation of river terrace sequences, *Neth. J. Geosci.*, *81*, 283–304.

Westaway, R. (2002b), Long-term river terrace sequences: Evidence for global increases in surface uplift rates in the late Pliocene and early middle Pleistocene caused by flow in the lower continental crust induced by surface processes, *Neth. J. Geosci.*, *81*, 305–328.

Westaway, R. (2002c), The Quaternary evolution of the Gulf of Corinth, central Greece: Coupling between surface processes and flow in the lower continental crust, *Tectonophysics*, *348*, 269–318.

Westaway, R. (2003), Kinematics of the Middle East and eastern Mediterranean updated, *Turkish J. Earth Sci.*, *12*, 5–46.

Westaway, R. (2004a), Kinematic consistency between the Dead Sea Fault Zone and the Neogene and Quaternary left-lateral faulting in SE Turkey, *Tectonophysics*, *391*, 203–237.

Westaway, R. (2004b), Review of "The steady-state orogen: Concepts, field observations, and models", edited by Frank Pazzaglia and Peter Knuepfer (special volume 151 of J. American Science, Yale Univ. Press, Connecticut, USA, 2001), *Am. J. Sci.*, *23*, 215–218.

Westaway, R. (2004c), Pliocene and Quaternary surface uplift revealed by sediments of the Loire-Allier river system, France, *Quaternaire*, *15*, 103–115.

Westaway, R., and J. Arger (2001), Kinematics of the Malatya-Ovacık Fault Zone, *Geodin. Acta*, *14*, 103–131.

Westaway, R., D. Maddy, and D. Bridgland (2002), Flow in the lower continental crust as a mechanism for the Quaternary uplift of south-east England: Constraints from the Thames terrace record, *Quat. Sci. Rev.*, *21*, 559–603.

Westaway, R., D. Bridgland, and S. Mishra (2003), Rheological differences between Archaean and younger crust can determine rates of Quaternary vertical motions revealed by fluvial geomorphology, *Terra Nova*, *15*, 287–298.

Westaway, R., M. Pringle, S. Yurtmen, T. Demir, D. Bridgland, G. Rowbotham, and D. Maddy (2004), Pliocene and Quaternary regional uplift in western Turkey: The Gediz river terrace staircase and the volcanism at Kula, *Tectonophysics*, *391*, 121–169.

Westaway, R., D. Bridgland, K. Challis, and M. White (2005a), A dating framework for the lower and middle Palaeolithic in Levantine rivers, *Counc. Br. Res. Levant Newslett.*, *2005*, 31–33.

Westaway, R., H. Guillou, S. Yurtmen, T. Demir, and G. Rowbotham (2005b), Constraints on the timing and regional conditions at the start of the present phase of crustal extension in western Turkey from observations in and around the Denizli region, *Geodin. Acta*, *18*, 313–343.

Westaway, R., T. Demir, A. Seyrek, and A. Beck (2006a), Kinematics of active left-lateral faulting in southeast Turkey from offset Pleistocene river gorges: Improved constraint on the rate and history of relative motion between the Turkish and Arabian plates, *J. Geol. Soc. London*, *163*, 149–164.

Westaway, R., H. Guillou, S. Yurtmen, A. Beck, D. Bridgland, T. Demir, S. Scaillet, and G. Rowbotham (2006b), Late Cenozoic uplift of western Turkey: Improved dating of the Kula Quaternary volcanic field and numerical modelling of the Gediz river terrace staircase, *Global Planet. Change*, *51*, 131–171.

Westaway, R., D. Bridgland, and M. White (2006c), The Quaternary uplift history of central southern England: Evidence from the terraces of the Solent

River system and nearby raised beaches, *Quat. Sci. Rev.*, *25*, 2212–2250.

Whiteman, C. A., and J. Rose (1992), Thames river sediments of the British early and middle Pleistocene, *Quat. Sci. Rev.*, *11*, 363–375.

Yurtmen, S., H. Guillou, R. Westaway, G. Rowbotham, and O. Tatar (2002), Rate of strike-slip motion on the Amanos Fault (Karasu Valley, southern Turkey) constrained by K-Ar dating and geochemical analysis of Quaternary basalts, *Tectonophysics*, *344*, 207–246.

Zor, E., E. Sandvol, C. Gürbüz, N. Türkelli, D. Seber, and M. Barazangi (2003), The crustal structure of the East Anatolian plateau (Turkey) from receiver functions, *Geophys. Res. Lett.*, *30*(24), 8044, doi:10.1029/2003GL018192.

A. Beck, School of Computing, University of Leeds, Leeds LS2 9JT, UK.

D. Bridgland, Department of Geography, Durham University, Durham DH1 3LE, UK.

T. Demir, Department of Geography, Harran University, 63300 Şanlıurfa, Turkey.

M. Pringle, Laboratory for Noble Gas Geochronology, Department of Earth, Atmospheric, and Planetary Sciences, Massachusetts Institute of Technology, Cambridge, MA 02139-4307, USA.

G. Rowbotham, School of Earth Sciences and Geography, Keele University, Keele ST5 5BG, UK.

R. Westaway, Faculty of Mathematics and Computing, Open University, Eldon House, Newcastle-upon-Tyne NE3 3PW, UK. (r.w.c.westaway@ncl.ac.uk)

S. Yurtmen, 41 Kingsway East, Westlands, Newcastle-under-Lyme ST5 5PY, UK.